Chapter 15

Wave Dispersion in Rods with a Rectangular Cross-section: Higher Order Theory and Experimentation

15.1. Introduction

Wave dispersion phenomena in rods have given rise to an abundance of literature. Higher order theories, using simple fields with three displacement components, have been presented with lengths for the three types of waves: torsional, bending and longitudinal. However, since 1920, longitudinal wave studies have shown that there are some weaknesses in the theories at the high frequency range. In this chapter, Touratier (see [TOU 79] and Chapter 7 in [CHE 10]) shows that, to fill this gap, it might be interesting to apply Hellinger–Reissner's theory using mixed fields of stress and displacement to satisfy all the possible boundary conditions. This is the price to pay to obtain satisfactory wave dispersion, particularly in the highest part of the frequency range. This chapter should be considered as complementary to Touratier's earlier work on theoretical formulations (see Chapter 7 in [CHE 10]). The main part of the chapter is devoted to experimental studies which allow the visualization of wave dispersions, not only in the highest frequency range but also for wave shapes in the thickness of the sample for higher elastodynamic modes. These modes have not been completely and experimentally explored, to our knowledge.

Chapter written by Maurice TOURATIER.

This chapter contains large extracts of Touratier's dissertation for his doctor-engineer degree, which was not prepared under the editors' supervision. His permission to publish this work is gratefully acknowledged.

Mechanical Characterization of Materials and Wave Dispersion: Instrumentation and Experiment Interpretation
Edited by Yvon Chevalier and Jean Tuong Vinh

Touratier's research seems at first sight academic but his experimental contributions open a new field of applications, particularly in experimental fracture mechanics. The proposed mechanical and electrical systems can easily be realized by experimenters in the laboratory, allowing the frequency domain beyond 100,000 Hertz to be explored, with special transducers which are not necessarily expensive to fabricate.

15.2. Summary table of some wave dispersion research

Space does not permit us to present an exhaustive critical study. Table 15.1 constitutes an abstract of the principal studies. Our attention is focused on rods with a finite length and rectangular cross-section. In Appendix 15A, Touratier's work is presented using Reissner's variational principle. This work is applicable to anisotropic materials with axial symmetry.

Authors	R.D. Mindlin [MIN 60]	E. Volterra [VOL 61]	A.D.S. Barr [BAR 62]	M.A. Medick [MED 66]	M. Touratier [TOU 79]
Essential points	Boundary conditions satisfied. Introduction of surface wave	Polynomial approximation for displacements. Shear weighting function. Boundary conditions partially satisfied (σ_{11} , σ_{22})	Displacement field. Weighting function.	Three field variational formulation. Weighting function	Double series of sine and cosine powers for displacement and stress field. Boundary conditions satisfied. Reissner formulation with two fields
Remarks	Exact solution for some values of a_1 and a_2	Original equations of motion	Original equations of motion	Volterra's equations of motion with weighting coefficient	Original equations of motion
Motion examined	Longitudinal motion coupled with radial shear	Longitudinal motion Transverse motion	Torsional motion	Longitudinal motion	Longitudinal, transverse and torsional motion
Applications	Infinity of modes Isotropic material	3 modes, isotropic material	2 modes in isotropic materials	Infinity of modes Isotropic material	Infinity of modes: anisotropic material with axial symmetry

Table 15.1. *Summary of various research on wave dispersion: a_1 and a_2 are width and thickness, respectively*

As this chapter is essentially devoted to applications, to be concise, details of the formulation of equations of motion are presented in Appendices 15A and15B.

15.3. Longitudinal wave dispersion: influence of the material and geometry of the bounded medium

For progressive wave propagation, displacement components are written as:

$$u_i^{mn}(x_3, t) = A_i \exp j\,(kx_3 - \omega t) \qquad [15.1]$$

This plane wave propagates along $\overrightarrow{x_3}$ axis with k being the wave number and ω the circular frequency. Bringing [15.1] into the equations of motion presented in Appendix 15A (equations [15.A.23] and [15.A.24]) and multiplying all the equation members by $a_1^2 S_{33}$, the frequency spectrum is obtained after transformation. The so-called dispersion relationship is obtained by equalizing the determinant of propagation equations to zero:

$$\det [\, e_{ij}(k, \omega)] = 0 \qquad [15.2]$$

with the following components of the dispersion matrix $[e_{ij}]$:

$$\left.\begin{aligned}
e_{11} &= \overline{\omega}^2 - \frac{64}{9\pi^2 s_{44}}\overline{k_1}^2 + \frac{\pi^2}{4\overline{\Delta}_E}\left(\frac{8s_{13}^2}{\pi^2} - s_{11}\right)\\
e_{12} &= \frac{2e}{\overline{\Delta}_E}\left(s_{11} - s_{13}^2\right) = e_{21}\\
e_{13} &= \frac{2js_{13}}{\overline{\Delta}_E}\left(s_{11} - \frac{8s_{12}}{\pi^2}\right)\overline{k_1} = -2e_{31}\\
e_{23} &= e\, e_{13} = -2e_{32}\\
e_{22} &= \overline{\omega^2} - \frac{64}{9\pi^2 s_{44}}\overline{k_1^2} + \frac{\pi^2 e^2}{4\overline{\Delta}_E}\left(\frac{8s_{13}^2}{\pi^2} - s_{11}\right)\\
e_{33} &= \overline{\omega^2} - \frac{\overline{k_1^2}}{\overline{\Delta}_E}\left(s_{11}^2 - \frac{64\, s_{12}^2}{\pi^2}\right)\\
e &= \frac{a_1}{a_2}\ \text{(flatness coefficient of the cross-section)}
\end{aligned}\right\} \qquad [15.3a]$$

$$\left.\begin{array}{ll} \overline{k_1} = 2\pi a_1 / \Lambda , & \text{where } \Lambda \text{ is the wavelength} \\ \overline{\omega^2} = \rho a_1^2 \omega^2 S_{33} , & \text{the circular frequency} \\ s_{ij} = S_{ij} / S_{33} , & \end{array}\right\} \quad [15.3b]$$

The lowercase s_{ij} designates the non-dimensional compliance matrix coefficient in equations [15.3a].

Numerical resolution (obtained by applying to the circular frequency (with real and positive values) is effected. This corresponds to the elastic problem without damping, while the complex wave number $\overline{k_1}$ (obtained by solving the determinantal dispersion equation) can be explained by the higher elastodynamic modes propagating with absorption of these waves in an elastic medium. These waves are injected in the rod wave guide. The phenomena gives rise to attenuated waves along the rod. We then have to deal with evanescent modes which are not due to the material (which is supposed to be elastic) itself.[1]

Let us focus our attention on the fact that the mathematical approximation adopted here is limited to the first order term in the series expansion of the three first elastodynamic modes of longitudinal wave propagation. These give rise to three distinct branches on the frequency spectrum drawn in the plane [ω (circular frequency) versus k (wave number)].

15.3.1. *Frequency spectrum*

The frequency spectrum is a graphical representation of the curve of a circular frequency ω versus the real part of the wave number, Re (k), or versus the imaginary part of k, Im (k). From this curve, the group velocity as well as the phase velocity can be evaluated. Remember, these two velocities are:

$v_p = \frac{\omega}{k}$ phase velocity

$v_g = \frac{d\omega}{dk}$ group velocity

1 This phenomenon is similar to the problem of Rayleigh's surface wave.

The relationship between v_p and v_g is:

$$v_g = v_p + k\frac{dv_p}{dk}$$

In the region where wave dispersion is weak, phase and group velocities are practically the same. In the region of the frequency spectrum where k is purely imaginary, the wave is evanescent, as mentioned above.

15.3.2. *Presentation of some frequency spectra regarding a boron fiber-aluminum composite*

Figure 15.1 shows that the first mode is weakly dispersive at a lower frequency. The low cut-off frequency corresponds to $\omega = 0$.

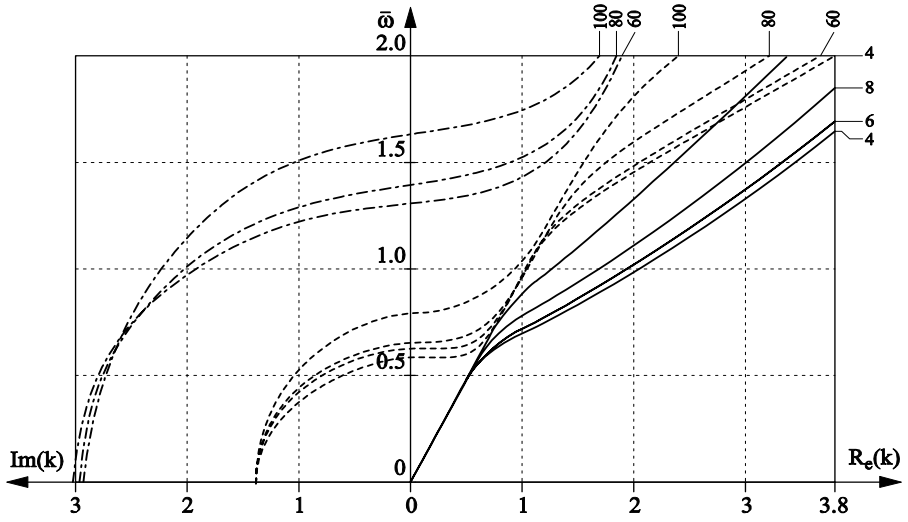

Figure 15.1. *Frequency spectrum for extensional vibration mode in a rod with rectangular cross-section, with flatness $e=a_1/a_2= 0.5$. Material: boron fiber–aluminum matrix. Volume percentage of fiber is indicated on curves. a_1 is half width and and a_2 is half thickness*

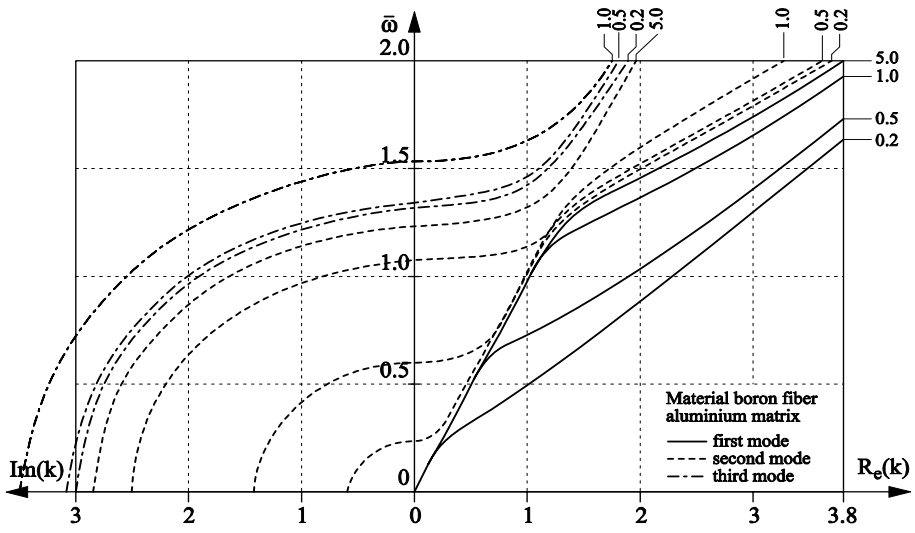

Figure 15.2. *Effect of flatness $=a_1/a_2$ (indicated on the curve.) on the frequency spectrum. Material: boron fiber-aluminum matrix. Continuous line = first mode, --- = second mode, -.-.-. = third mode. a_1 is the half width and a_2 is the half thickness of the rod*

A longitudinal wave propagates without restriction for $\omega \neq 0$. Figure 15.2 shows the influence of flatness (the ratio of width to thickness) on the frequency spectrum. The phase velocity is strongly dependent on flatness.

The second and third elastodynamic modes have a lower cut-off frequency corresponding to the intersection of the curves with a real axis ω before entering in the region of imaginary values of the wave number.

Touratier's method gives rise to faster convergence even with a first order approximation.

For comparison with existing theories, an isotropic material was adopted, with a rod of square cross-section and Poisson's number $\nu = 0.3$. This constitutes the main interest of Hellinger–Reissner's mixed fields formulation.

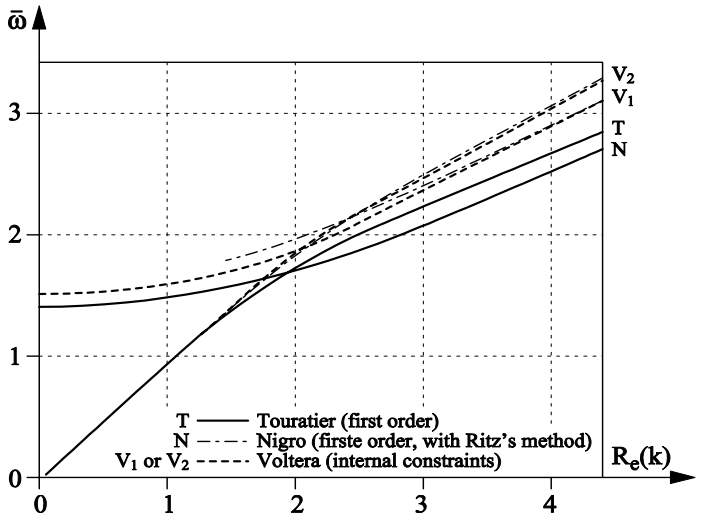

Figure 15.3. *Comparison of three theories for a frequency spectrum with longitudinal modes: T = Touratier (first order), N = Nigro (first order, with Ritz's method), - - - = Volterra (with internal constraints: V, first mode and ,V_2, second mode)*

15.4. Bending wave dispersion

Section 15A.25 in Appendix 15A gives equations of motion. If an attempt is made to uncouple these equations, we obtain a *sixth order equation of motion* in which F designates any of the three displacement components (u_1^{11}, u_2^{00}, u_3^{01}):

$$+ f1 \; + f2 \; + f3 \; + f\,4 \; + f6 \; + f\,7 \; + f\,8 \; = 0$$

$$-\frac{\partial^6 F}{\partial t^6} + f_1 \frac{\partial^4 F}{\partial t^4} + f_2 \frac{\partial^2 F}{\partial t^2} + f_3 \frac{\partial^6 F}{\partial x_3^6} + f_4 \frac{\partial^4 F}{\partial x_3^4} + f_5 \frac{\partial^2 F}{\partial x_3^2} + f_6 \frac{\partial^6 F}{\partial t^4 \partial x_3^2} + f_7 \frac{\partial^6 F}{\partial t^2 \partial x_3^4} + f_8 \frac{\partial^4 F}{\partial t^2 \partial x_3^2} = 0$$

[15.4]

15.4.1. *Upper bound for phase velocities*

Using a progressive wave:

$$F(x_3, t) = B \exp[\, jk(x_3 - ct)] \qquad [15.5]$$

with frequency tending to infinity, wave velocity reaches the following limit for a pure bending wave (equation [15.A.29]):

$$\overline{c_\infty^6} = \frac{512}{9\pi^4 s_{44}^2 \overline{\Delta_F}} \left(s_{11}^2 - \frac{512 s_{12}^2}{9\pi^4}\right)$$

Front wave velocities are (equation [15.A.29]):

$$\overline{c_{1\infty}} = \frac{8}{3\pi\sqrt{s_{44}}} \; ; \; \overline{c_{2\infty}} = \frac{\sqrt{8}}{\pi\sqrt{s_{44}}} \; ; \; \overline{c_{3\infty}} = \sqrt{\frac{1}{\overline{\Delta_F}}} \left(s_{11}^2 - \frac{512}{9\pi^4} s_{12}^2\right)^{1/2} \qquad [15.6]$$

with $s_{ij} = S_{ij}/S_{33}$; $\overline{\Delta_F} = \Delta_F / S_{33}^2$, $\overline{c^2} = \rho S_{33} c^2$.

The term in [15.4] with the lowest degree gives the lower bound for velocity $\overline{c_6^2} = 0$.

Note: the first order approximation of bending motion permits phase velocities to be reached with the following levels of accuracy:

5% between $c_{1\infty}$ and the exact value c_R (Rayleigh velocity);

10% between $c_{2\infty}$ and the exact value c_T (shear wave velocity);

40% between $c_{3\infty}$ and the exact value c_T (shear wave velocity).

15.4.2. *Dispersion of bending wave: the influence of various characteristics*

The dispersion relationship is obtained from the following matricial equation:

$$\det [f_{ij}] = 0 \qquad [15.7]$$

with the following coefficients:

$$\left.\begin{aligned} f_{11} &= \overline{\omega^2} - \frac{64}{9\pi^2 s_{44}} \overline{k_1^2} - \frac{\pi^2}{4\overline{\Delta_F}} \left(s_{11} - \frac{64 s_{13}^2}{9\pi^2}\right) - \frac{16 e^2}{9 s_{66}} \\ f_{12} &= f_{21} = 0 \\ f_{13} &= -\frac{2j s_{13}}{\overline{\Delta_F}} \left(\frac{64 s_{12}}{9\pi^2} - s_{11}\right) \overline{k_1} = -2 f_{31} \quad \text{with } j = \sqrt{-1} \\ f_{22} &= \overline{\omega}^2 - \frac{8}{\pi^2 s_{44}} \overline{k_1}^2 \end{aligned}\right\} \qquad [15.8a]$$

$$f_{23}= \frac{je}{s_{44}} \bar{k_1} = -\frac{1}{2} f\,32 \quad \text{with } j=\sqrt{-1}$$

$$f_{33}= \bar{\omega}^2 - \frac{1}{\bar{\Delta_F}}\left(s_{11}^2 - \frac{512}{9\pi^4} s_{12}^2 \right) \bar{k_1}^2 - \frac{\pi^2}{4 s_{44}} e^2 \qquad [15.8b]$$

$$\bar{k_1} = k a_1; \quad \bar{\omega}^2 = \rho a_1^2 \omega^2 S_{33} \; ; \quad e = \frac{a_1}{a_2}$$

$$\bar{\Delta_F} = \Delta_F / S_{33}^2 \; ; \quad s_{ij} = S_{ij} / S_{33} \qquad [15.8c]$$

With regard to the compliance matrix coefficients S_{ij}, for a composite boron fiber -aluminum matrix, and for a given percentage volume of fiber, it is possible to evaluate S_{ij} using previsional calculations of the transverse isotropic composite; see [CHE 75].

By bringing S_{ij} into [15.8], all the f_{ij} coefficients can be numerically evaluated. Solving [15.7] allows the frequency spectrum to be obtained.

15.4.3. *Frequency spectrum for a bending wave*

Figure 15.4 shows the frequency spectrum for the boron fiber-aluminum composite matrix indicated above. The following remarks can be made:

– the spatial attenuation of the bending wave is small compared to that of an extensional wave. The spectra with imaginary parts of the wave number as abscissa (which concern only the higher modes and not the first elastodynamic mode), are presented in Figures 15.4 and 15.5;

– the phase velocity increases with the frequency for the first mode;

– the wave dispersion is more pronounced for a higher percentage volume of fiber.

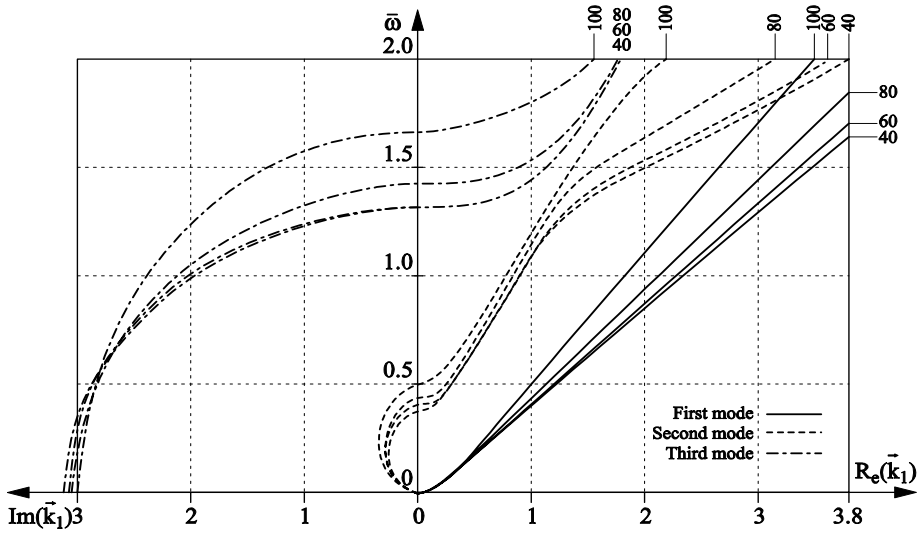

Figure 15.4. *Frequency spectrum of a bending wave (material: boron fiber–aluminum matrix). The transverse isotropic material is e = a_2/a_1. Percentage volume p is indicated on each curve. Continuous line = first mode; --- = second mode; -. -. - (mixed lines/dots) = third mode*

15.4.4. *Influence of flatness e = a_1/a_2*

The frequency spectrum for the same material is presented for various values of p, the percentage volume of fiber, in Figure 15.5. When e increases, the dispersion is more pronounced, particularly for the first mode.

By contrast, for the second and the third modes, dispersion is less pronounced as flatness e increases. This can be attributed to the intervention of longitudinal components along axis $O\overrightarrow{x_1}$ of the displacement which are predominant in higher modes.

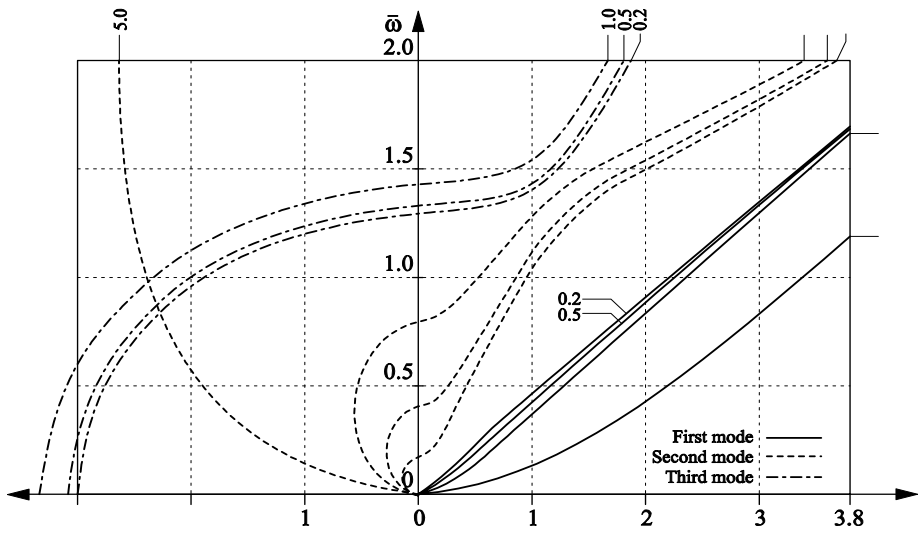

Figure 15.5. *Influence of flatness $e=a_1/a_2$ on the frequency spectrum of bending wave. Material: boron fiber-aluminum matrix, transverse isotropic material. First mode ---- continuous line; Second mode interrupted line -. -. -. -; Third mode mixed lines and dots. a_1 half thickness, a_2 half width*

15.4.5. *Comparison between various theories*

We examined an isotropic material with Poisson's number $\nu = 0.3$ and with flatness $e = a_1/a_2 = 2$. Touratier [TOU 79] used Reissner's variational principle up to the tenth order for the displacement field.

Figure 15.6 shows that in a frequency spectrum representation, for a bending fundamental mode, there is agreement between his theory with those proposed by S.P. Timoshenko [TIM 21] and N.J. Nigro [NIG 68] amongst others, at least for the first elastodynamic modes.

By contrast, Nigro's and Timoshenko's theories give poor convergence. The reason for this is the low degree of equations of motion adopted by these authors.

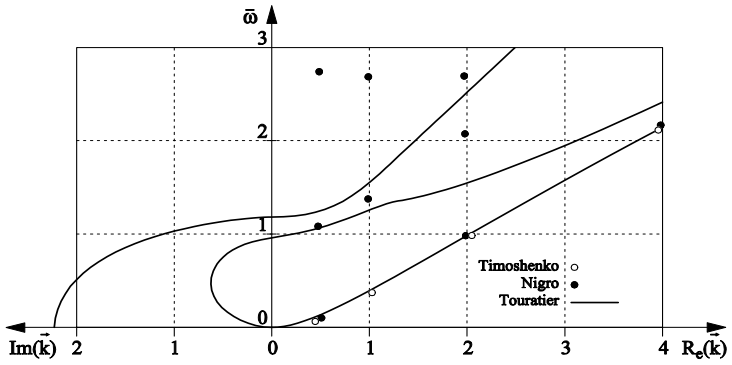

Figure 15.6. *Bending frequency spectrum of a rod with a rectangular cross-section. Material: composite boron fiber-aluminum matrix. Percentage volume of fiber: 60%. Flatness: e= a_1/a_2=2-*

A second observation concerns Nigro's theory which uses a simple displacement field. Although the series is expanded to ten terms, convergence is poor for the second mode; the main reason being essentially that boundary conditions are not fully satisfied.

15.5. First order for torsional motion in a transverse isotropic rod

15.5.1. *Equations of motion*

Series expansion is limited to the first term. The displacement field is $0\overrightarrow{x_3}$, the axis of the rod being the symmetrical axis of the transverse isotropic material:

$$\vec{u}\ (M,t) = \sin\frac{\pi\varphi_1}{2}\ u_1^{01}\overrightarrow{x_1} + \sin\frac{\pi\varphi_2}{2}\,u_2^{10}\overrightarrow{x_2} + \sin\frac{\pi\varphi_1}{2}\sin\frac{\pi\varphi_2}{2}\,u_3^{11}\overrightarrow{x_3} \qquad [15.9]$$

with $\varphi_i = \frac{x_i}{a_i}$

The matricial form of stress field is:

$$[\,\sigma\,] = \begin{pmatrix} \frac{1}{2}\sin\frac{\pi}{2}\varphi_1\sin\frac{\pi}{2}\varphi_2.\,\sigma_{11}^{11} & \cos\frac{\pi\varphi_1}{2}\cos\frac{\pi\varphi_2}{2}\,\sigma_{12}^{00} & \cos\frac{\pi\varphi_1}{2}\sin\frac{\pi\varphi_2}{2}\,\sigma_{31}^{01} \\ \cos\frac{\pi\varphi_1}{2}\cos\frac{\pi\varphi_2}{2}\,\sigma_{12}^{00} & \frac{1}{2}\sin\frac{\pi\varphi_1}{2}\sin\frac{\pi\varphi_2}{2}\,\sigma_{22}^{11} & \sin\frac{\pi\varphi_1}{2}\cos\frac{\pi\varphi_2}{2}.\sigma_{23}^{10} \\ \cos\frac{\pi\varphi_1}{2}\sin\frac{\pi\varphi_2}{2}\,\sigma_{31}^{01} & \sin\frac{\pi\varphi_1}{2}\cos\frac{\pi\varphi_2}{2}\,\sigma_{23}^{10} & \sin\frac{\pi\varphi_1}{2}\sin\frac{\pi\varphi_1}{2}\,\sigma_{33}^{11} \end{pmatrix} \qquad [15.10]$$

The equations of motion deduced from [15.9 and 15.10] are, with the degree of time derivative designated (after a comma) by the number of letter t's in the subscript, with the first member and space derivative after a comma in subscripts with respect to coordinate 3 in the second member:

$$\left.\begin{aligned}
\rho\ddot{u}^{01}_{1,tt} &= \frac{2}{\pi}\sigma^{01}_{31,3} - \frac{1}{a_2}\sigma^{00}_{12} \\
\rho\ddot{u}^{10}_{2,tt} &= \frac{2}{\pi}\sigma^{10}_{23,3} - \frac{1}{a_1}\sigma^{00}_{12} \\
\rho\ddot{u}^{11}_{3,tt} &= \sigma^{10}_{33,3} - \frac{\pi}{2a_2}\sigma^{10}_{23} - \frac{\pi}{2a_1}\sigma^{01}_{31}
\end{aligned}\right\} \qquad [15.11]$$

Constitutive equations for the material give, using a letter after a comma to notate the derivative with respect to the variable before the comma:

$$\left.\begin{aligned}
&S_{11}\sigma^{11}_{11} + \frac{64}{9\pi^2}\sigma^{11}_{22} + \frac{16}{3\pi}S_{13}\sigma^{11}_{33} = 0 \\
&\frac{64}{9\pi^2}\sigma^{11}_{11} + S11\sigma^{11}_{22} + \frac{16}{3\pi}S_{13}\sigma^{11}_{33} = 0 \\
&\frac{4}{3\pi}S_{13}\,\sigma^{11}_{11} + \frac{4}{3\pi}S13\,\sigma^{11}_{22} + S_{33}\sigma^{11}_{33} = u^{11}_{3,3} \\
&\sigma^{10}_{23} = \frac{4}{\pi S_{44}}u^{10}_{2,3} + \frac{\pi}{2a_2 S_{44}}u^{11}_{3} \\
&\sigma^{01}_{31} = \frac{4}{\pi S_{44}}u^{01}_{1,3} + \frac{\pi}{2a_1 S_{44}}u^{11}_{3} \\
&\sigma^{00}_{12} = \frac{2}{S_{66}}\left(\frac{1}{a_2}u^{01}_{1} + \frac{1}{a_1}u^{10}_{2}\right)
\end{aligned}\right\} \qquad [15.12]$$

Bringing [15.12] and [15.10] into [15.11] we obtain equations of motion expressed only with displacement components:

$$\left.\begin{aligned}
\rho\ddot{u}^{01}_{1,tt} &= \frac{8}{\pi^2 S_{44}}u^{01}_{1,33} - \frac{2}{a_2^2 S_{66}}u^{01}_{1} - \frac{2u^{10}_{2}}{a_1 a_2 S_{66}} + \frac{1}{a_1 S_{44}}u^{11}_{3,3}\\
\rho\ddot{u}^{10}_{2,tt} &= \frac{8}{\pi^2 S_{44}}u^{10}_{2,33} - \frac{2}{a_1^2 S_{66}}u^{10}_{2} - \frac{2}{a_1 a_2 S_{66}}u^{01}_{1} + \frac{1}{a_2 S_{44}}u^{11}_{3,3}\\
\rho\ddot{u}^{11}_{3,tt} &= \frac{1}{\Delta_T}\{S^2_{11} - \left(\frac{64S_{12}}{9\pi^2}\right)2\}u^{11}_{3,33} - \frac{\pi^2}{4S_{44}}\left(\frac{1}{a_1^2}+\frac{1}{a_2^2}\right)u^{11}_{3}\\
&\qquad - \frac{2}{a_1 S_{44}}u^{01}_{1,3} - \frac{2}{a_2 S_{44}}u^{10}_{2,3}
\end{aligned}\right\} \qquad [15.13]$$

$$\text{with } \Delta_T = (S_{11} - \frac{64S_{12}}{9\pi^2})\ \{S_{13}(\frac{64S_{12}}{9\pi^2} + S_{11}) - \frac{128S_{13}^2}{9\pi^2}\} \qquad [15.14]$$

15.5.2. *Physical interpretation of displacement components*

The following comments are of interest for further applications:

– term $\ddot{u}^{11}{}_3$ is associated with inertia correction along the axis $0\overrightarrow{x_3}$. The term $\ddot{u}^{11}_{3,33}$ describes longitudinal stress, whilst $u_3{}^{11}$ is a warping term;

– terms $\ddot{u}_{1,33}{}^{01}$ and $\ddot{u}_{233}{}^{10}$ concern shear effects;

– functions $u_1{}^{01}$, $u_2{}^{10}$ and $u_3{}^{11}$ are related to three modes of torsional motion to which drawings in Figure 15.7(a) and (b) are associated;

– it is useful to return to Saint Venant's theory of torsion to discuss the warping of the cross-section. The longitudinal component of displacement is written as:

$$w(z,t) = u_3(x_3,t) = \phi(x_1, x_2)\ \zeta\ (x_3, t) \qquad [15.15]$$

where $w = u_3$, $u = u_1$ and $v = u_2$.

This equation gives rise to the Laplace equation. Barr retained Saint Venant's expression. Engstrom has shown that the cross-section warping function is a Helmholtz's equation [NUG 77], and this equation is time dependent. Comparing the longitudinal displacement component u_3 suggested above by Barr and Engstrom, the same component in Touratier's theory is:

$$u_3 = \sum_{p,q\geq 0} \sin^{2p+1}\frac{\pi}{2}\phi_1 .\ \sin^{2q+1}\frac{\pi}{2}\phi_2\ .u_3^{2p+1,2q+1}(x_3,t) \qquad [15.16]$$

We notice that [15.16] takes warping into account in the product of the two first terms of the second member and u_3 is frequency dependent. However, the warping effect does not explicitly appear. This constitutes a simple method which takes into

account the warping effect. This effect changes simply with the elastodynamic mode.

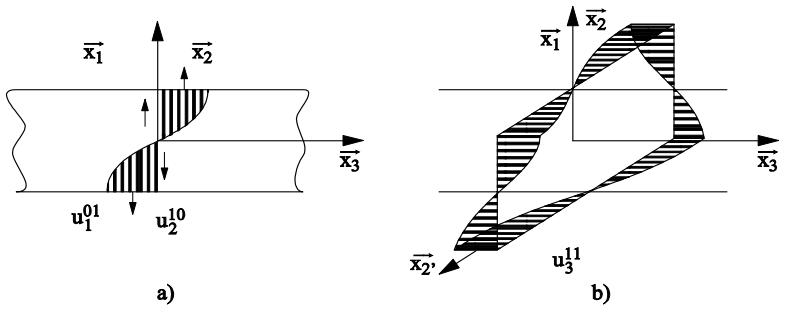

Figure 15.7. *Displacement components in torsional motion*
(a) influence of rotational inertia b) warping phenomena which creates distorsion of the cross-section

15.5.3. *Asymptotic values of phase velocities*

The three equations of motion [15.13] can be reduced to just one by eliminating the other variables:

$$-\frac{\partial^6 T}{\partial t^6} + t_1 \frac{\partial^4 T}{\partial t^4} + t_2 \frac{\partial^2 T}{\partial t^2} + t_3 \frac{\partial^6 T}{\partial x_3^6} + t_4 \frac{\partial^4 T}{\partial x_3^4} + t_5 \frac{\partial^2 T}{\partial x_3^2} + t_6 \frac{\partial^6 T}{\partial t^4 \partial x_3^2} + t_7 \frac{\partial^6 T}{\partial t^2 \partial x_3^4} + t_8 \frac{\partial^4 T}{\partial t^2 \partial x_3^2} = 0 \qquad [15.17]$$

in which T designates any function among the three displacement components (u_1^{01}, u_2^{10}, u_3^{11}). The upper limits for velocities are $c_\infty^6 = t_3$, t_3 being a coefficient in [15.17].

With reduced variables (equations [15.A.27])

$$c_\infty^6 = \frac{64}{\pi^4 s_{44}^2 \overline{\Delta_T}} \{s_{11}^2 - (\frac{64 s_{12}}{9\pi^2})^2\} \qquad [15.18]$$

from which the following asymptotic values of phase velocities are obtained:

$$\overline{c_{1\infty}} = \overline{c_{2\infty}} = \frac{1}{\pi}\sqrt{\frac{8}{s_{44}}}\,\overline{c_{3\infty}} = \sqrt{\frac{1}{\Delta_T}}\{s_{11}^2 - (\frac{64 s_{12}}{9\pi^2})^2\}^{1/2} \qquad [15.19]$$

For an isotropic material with Poisson's coefficient $\nu = 0.3$, the following discrepancies are obtained:

$\overline{c_{1\infty}} \cong \overline{c_R}$ no discrepancy for fundamental mode;

$\overline{c_{2\infty}} \cong \overline{c_R}$ 10% discrepancy for second mode;

$\overline{c_{3\infty}} \cong 1$ 40% discrepancy for third mode.

The effective front wave velocity is given by:

$c_0^2 = -t_5/t_2$, t_5 and t_2 being coefficients of equation [15.17], giving the asymptotic values of phase velocities (upper limits), or:

$$\overline{c_0} = \frac{e}{\pi(1+e^2)}\sqrt{\frac{8(3+e^2)}{s_{44}}}\;; \quad e=\frac{a_1}{a_2} \qquad [15.20]$$

Formula [15.20] shows that if e=1 (square cross-section) we find $\overline{c_0} \cong \overline{c_R} \cong \overline{c_1}$.

The square cross-section is interesting from an experimental point of view. In many circumstances, the corresponding wave dispersion is nearly that of a circular cross-section.

If $e \neq 1$, the value of $\overline{c_0}$ depends on the flatness, e. Only a torsional wave presents this specific property.

15.5.4. *Torsional wave dispersion: influence of the material and the geometry of the medium*

Displacement components are expressions of plane progressive waves. The frequency spectrum equation is:

$$\det[t_{ij}] = 0 \qquad [15.21]$$

The components t_{ij} of coefficients in [15.17] are presented below:

$$\left.\begin{aligned}
t_{11} &= \overline{\omega}^2 - \frac{8}{\pi^2 s_{44}}\overline{k_1}^2 - \frac{2e^2}{s_{66}} \\
t_{12} &= -\frac{2e}{s_{66}} = t_{21} \\
t_{13} &= j\overline{k_1}/\,s_{44} = -\frac{1}{2}t_{31} \\
t_{23} &= e\,t_{13} = -\frac{1}{2}t_{32} \\
t_{22} &= \overline{\omega}^2 - \frac{8}{\pi^2 s_{44}}\overline{k_1}^2 - \frac{2}{s_{66}} \\
t_{33} &= \overline{\omega}^2 - \frac{1}{\Delta_F}\left\{ s_{11}^2 - \left(\frac{64 s_{12}}{9\pi^2}\right)^2\right\}\overline{k_1}^2 - \frac{\pi^2(1+e^2)}{4 s_{44}}
\end{aligned}\right\} \qquad [15.22a]$$

$$\left.\begin{array}{l} \overline{\Delta_T} = \Delta_T / S_{33}^2 \;\; ; \;\; e = \frac{a_1}{a_2} \\ s_{ij} = \frac{S_{ij}}{S_{33}} \;\; ; \;\; \bar{\omega}^2 = \rho a_1^2 \omega^2 S_{33} \;\; ; \;\; \overline{k_1} = 2\pi a_1 / \Lambda \end{array}\right\} \qquad [15.22b]$$

15.5.5. *Frequency spectrum for torsional waves*

Figure 15.8 shows the frequency spectrum for a rod with a rectangular cross-section, the material being an anisotropic composite with a boron fiber-aluminum matrix. The fiber percentage is indicated on each curve.

15.5.5.1. *Characteristics of torsional waves*

For the first mode, the relative wave number $\overline{k_1}$ is complex, as is the case for longitudinal and bending waves.

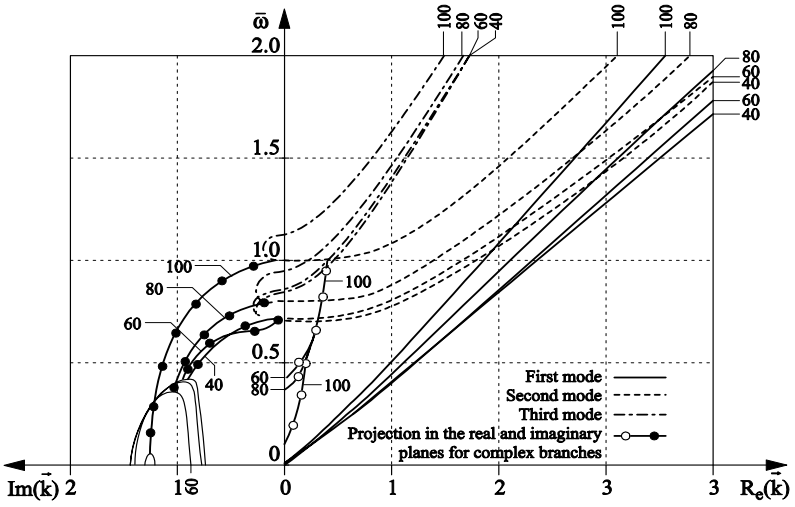

Figure 15.8. *Frequency spectrum for a torsional wave; rod with a rectangular cross-section; material: boron fiber-aluminum composite matrix. Flatness e =a_1/a_2= 0.5. Continuous line - first mode; dotted line - - - second mode; alternate line and dots · — · third mode,with projections in the real and imaginary planes for complex branches*

The decrease in percentage volume of fibers is accompanied by an accentuation of wave dispersion for the three examined modes. Figure 15.8 describes the influence of the flatness parameter, e, on the frequencies associated with the first three modes for a percentage fiber volume of 60%.

For the first mode, if $e = a_1/a_2 \leq 1$, the dispersion is weak, particularly when e = 1 (for a square section). It is less sensitive to the variation of e than for longitudinal motion.

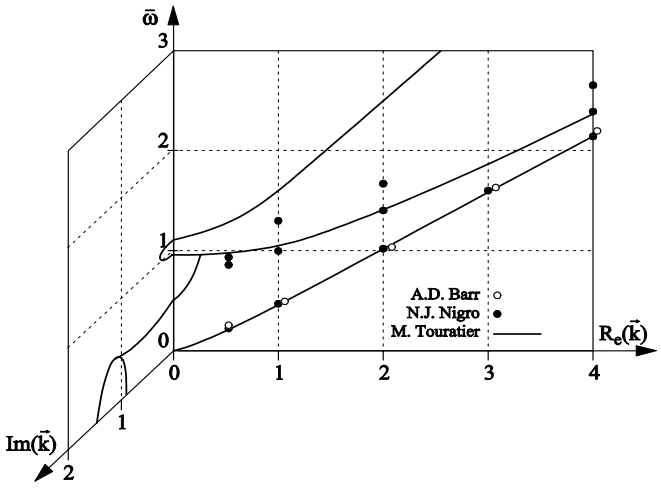

Figure 15.9. *Comparison between three theories of torsion applied to an isotropic material with Poisson's number $\nu = 0.3$. Rectangular cross-section with $e = a_1/a_2 = 0.5$.*
° ° ° = A.D. Barr; ●●● = N.J. Nigro; ----- = Touratier

15.5.6. *Comparison with other theories*

The material is isotropic with Poisson's number $\nu = 0.3$. Touratier's theory is compared to Nigro's theory. Figure 15.9 collects the three groups of results.

For the first elastodynamic mode with e = 0.5 the three theories give practically the same results. For the second mode, although Touratier's theory presented above is of the first order, it gives more satisfactory results than Nigro's theory. Remember that this last theory uses ten terms in the series expansion of displacement components. Barr's theory is presented only for the first mode.

15.6. Interest in theories with higher degrees of approximation

In Appendix 15A, a higher degree approximation is utilized by Touratier [TOU 79] to study up to nine first elastodynamic modes.

We focus our attention here on the practical aspects of wave dispersions concerning the three types of waves.

15.6.1. *Choice of appropriate theory for application in the characterization of viscoelastic materials*

If we are interested in this type of application, the first elastodynamic modes for the three types of waves are sufficient. However, the degree of decoupled equations of motion has an influence on the accuracy of the dispersion curves, particularly at a higher frequency.

15.6.1.1. *Practical remarks about longitudinal waves*

For Bishop's equation of motion, Nugues (see Chapter 5 in [CHE 10]) indeed affords some improvements with respect to elementary equations at medium frequency. But at a higher frequency, this equation is unable to portray dispersion curves correctly. A comparative study of wave dispersion curves is interesting and allows the appropriate theory to be chosen in a given interval of frequencies. Experimenters must have in mind the principal parameters which have an important influence on the trend of the dispersion curve:

– the flatness, e, which characterizes the cross-section;

– for composite anisotropic materials, the ratio of shear modulus to the Young's longitudinal modulus constitutes an important factor which strongly influences the wave dispersion;

– observation of Bishop's and Touratier's curves permits the appropriate theory to be chosen. Eventually the coincidence of the two curves helps us to determine the maximum frequency for which Bishop's theory is valid for the first elastodynamic mode;

– if the exploration of the frequency interval goes beyond the aforementioned upper frequency, Touratier's theories might be more appropriate.[2]

15.6.1.2. *Practical remark about bending waves*

Mindlin's theory is appropriate for utilization at the first elastodynamic mode.[3]

15.6.1.3. *Practical remarks about torsional waves*

A preliminary comparative study is necessary. The following theories have to be examined[4]: Saint Venant's theory at the lowest frequency range (the Improved Saint Venant's Theory (Barr's theory), with frequency dependent warping (Chapter 5), is

2 Remember that Touratier proposed a theory using simple field of displacement which is the extension of Volterra's theory to composite materials (see Chapter 7 [CHE 10]).
3 A bending wave is the only one which necessitates fourth order theory to cover higher frequency ranges up to the asymptotic Rayleigh's velocity.
4 If possible, use non-dimensional variables: frequency, velocity, slenderness and flatness.

good. If Barr's theory is not appropriate at a medium or higher frequency, Touratier's theory (presented in this chapter) might be useful.

15.6.2. *Interest in elastodynamic modes higher than fundamental ones*

Higher elastodynamic modes are used with success in ultrasonics and piezoelectric waveguides. We notice that, in some cases, waves propagate with higher energy than which occurs in the first elastodynamic mode.

If the frequency spectrum is examined at higher modes, parts of the frequency spectrum correspond to real values of wave number k. This means that waves propagate without attenuation. This property is exploited in piezoelectric wave guides.

15.6.2.1. *Defect size*

One of the possible applications is in defect detection in materials when the defects are of small size. With the dispersion curves presented above in view, if the size of a defect is of the order of the wave length, Λ, a progressive wave at high frequency crossing the defect has its shape modified by the defect itself.

15.6.2.2. *Defect localization*

Ultrasonic defect control is already a well-known field. The difference here is that, for defect localization, special transducers not yet commercially available are required; the frequency and size of such transducers are for the moment unusual but they are realizable in practice.

15.7. Experimental set-ups to visualize stationary waves in rods

This section presents mechanical and electronic set-ups which can be easily realized.[5] In Chapter 11, experimental set-ups were devoted to longitudinal fundamental (first) modes. This section presents not only fundamental modes but also higher vibration elastodynamic modes with the aim of a confrontation between theory and experimentation.

5 They can be used as laboratory work for students to illustrate an advanced course on elastodynamics. The same set-up can also be used for material characterization.

15.7.1. *Choice and fabrication of special transducers and exciters*

As the working frequency may be high and reaches the ultrasonic frequency range, the electrodynamic exciter (shaker) is replaced by special piezoelectric or ferroelectric transducers. These transducers are specially designed and built for utilization in special ultrasonic benches. Their weights and volumes are reduced so that their presence at the sample free ends can be considered negligible. The total surfaces of the transducers are that of the sample cross-section. When these transducers are glued at the free ends of the rod, their weight contributes to lower the resonance frequency of the stationary waves if the rod length is short. In practice, the ratio (mass of the transducers at one end/rod mass) is to be taken into account. If the ratio is small, much less than 1/50, the end sample is assimilated to a free end.

In Chapter 4, the functioning principles of ferroelectric transducers[6] were presented in detail concerning practical utilization. Let us recall here the basic ideas.

15.7.1.1. *Polarization*

Both the polarization vector $\overrightarrow{D}$ and the mechanical vibration vector $\vec{e}$ are not necessarily collinear (see Figure 4.19 of Chapter 4).

For a longitudinal (axial) vibration of a rod, the two vectors $\vec{D}$ and $\vec{e}$ are collinear. In ceramic plates, vibration is created by the change of thickness in the direction o$\overrightarrow{x_3}$ of the rod (second and third column of Table 4.15, Chapter 4).

For transverse (shear wave) vibration, a ceramic plate with $\vec{D}$ orthogonal to $\vec{e}$ should be chosen.

15.7.1.2. *Size of transducer*

Figure 15.10 shows one single emitter which produces longitudinal motion in a rod.

15.7.1.2.1. Longitudinal vibration of a rod with ferroelectric transducer to create the first mode

The choice of the number of transducers depends on the profile of the displacement in the cross-section we wish to obtain; see Figure 15B.1. 15B.1(a) corresponds to one transducer, whereas 15B.1(b) requires two transducers. If possible, the height of the transducer chosen is equal to the thickness of the rod.

---

6 A ferroelectric transducer is preferred to a piezoelectric one because large ferroelectric plates with various thickness are commercially available and a latitude of choice of ferroelectric parameters is possible.

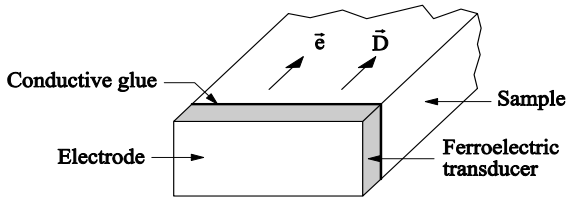

Figure 15.10. *Ceramic ferroelectric transducers tailored to the plate, serving as emitter which produces longitudinal (extensional) stationary vibration in the rod*

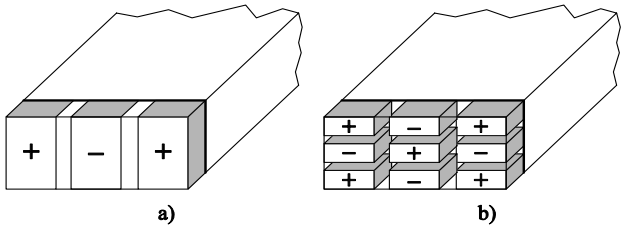

Figure 15.11. *Positioning of special ferroelectric transducers on the surface of the sample free end section. (a) Three small rectangular transducers cut from a large ferroelectric plate and glued at one free end; (b) nine small rectangular ferroelectric emitters used to obtain a more complicated profile of emitter waves (see Figure 15B.1)*

15.7.1.2.2. Longitudinal vibration of rod to create elastodynamic mode order higher than one

It is possible to create a wave profile in the whole section with many nodes and antinodes. Figure 15.11(a) shows profiles with two nodal lines and two peaks separated by one trough in the middle. Figure 15.11(b) shows nine pavements which allow nine zones to be obtained over the whole sample, with alternate peaks and troughs across the width as well as across the thickness.

15.7.1.2.3. Electric isolation of adjoining zones between pavements

It is necessary to electrically isolate these zones to ensure the wave profiles at higher elastodynamic modes.

15.7.1.2.4. Rod bending motion

The ferroelectric plates are presented in section 4.7.4 (Chapter 4 shows that it is easy to choose polarization vector $\vec{D}$ and orthogonal vibration direction $\vec{e}$ orthogonal, see Table 4.3). For bending motion in a rod, the experimenter has to choose bending motion either in the direction of thickness or the direction of width. Figure 15.12 indicates the positioning of the ferroelectric plates.

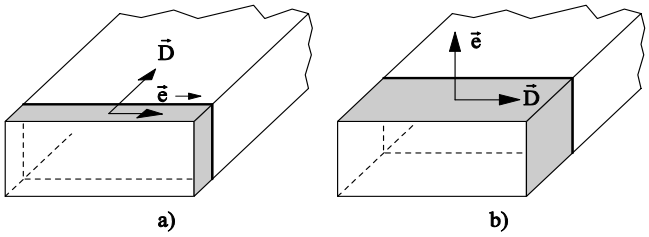

Figure 15.12. *Bending motion in the fundamental elastodynamic mode. (a) Horizontal bending motion, direction $\vec{e}$ orthogonal to polarization $\vec{D}$, oriented in the direction of rod axis $O\vec{z}$; (b) Vertical bending motion, polarization $\vec{D}$ is in the horizontal direction, $\vec{e}$ bending motion is vertical*

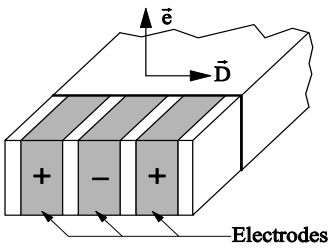

Figure 15.13. *Ferroelectric emitter constituted of three transducers to produce higher elastodynamic mode in bending. $\vec{D}$, polarization vector, and displacement vector, $\vec{e}$, are orthogonal. Transducers are realized to create vibration and to measure horizontal bending motion*

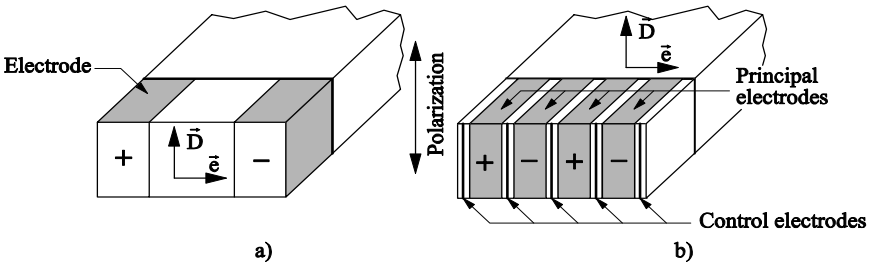

Figure 15.14. *An even number of ferroelectric transducers is necessary to create torsional motion. (a) Shear motion in first elastodynamic mode; (b) higher elastodynamic shear mode with an even number of transducers*

15.7.1.2.5. Rod torsional motion

For symmetric shear motion, an even number of ferroelectric plates is adopted, see Figure 15.14.

15.7.2. *Mechanical and electrical operations on ferroelectric transducers*

Cutting, milling and gluing operations are necessary after the choice of the rod sample.

15.7.2.1. *Cutting of small transducers*

From a ferroelectric plate, any cutting of small transducers should be done with caution to avoid breaking the fragile ferroelectric plate.

15.7.2.2. *Milling*

This operation is necessary to obtain transducer dimensions with sufficient accuracy.

15.7.2.3. *Micro-sanding*

Instead of cutting small transducers, a ferroelectric rectangular plate can be realized which has the surface of the whole cross-section. On this plate, an array of transducers is realized. The first operation consists of masking the surfaces of future principal electrodes which are distributed regularly on the rectangular plate. By micro-sanding the non-protected surfaces, the metallic coating is removed. Thus, isolated surfaces are created periodically, see Figure 15.15.

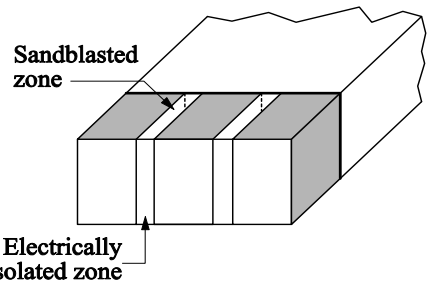

Figure 15.15. *Emitter and receiver transducers for extensional waves*[7]*. Creation of array of transducers by micro-sanding. The whole transducer array occupies the entire cross-section*

7 This figure is just an example. For a shear wave and bending waves, the two aforementioned vectors must be correctly oriented so as they are orthogonal (Chapter 4, section 4.7).

15.7.2.4. *Electric connections*

Two kinds of electrodes are to be realized: electrodes to create polarization $\overrightarrow{D}$, and control electrodes in the sand blasted narrow zones between transducers in the array which ensure, during tests, that the polarity of obtained waves (vector $\vec{e}$) are correct. For the control electrodes, a conducting glue is used with fine electrical wires.

15.7.3. *Gluing the isolated transducer and transducer array*

Caution is necessary for this operation. The glue used must be non-conducting and the glue layer must be as thin as possible. This operation is definitive and repair is difficult or even impossible after glue drying.

15.8. Electronic set-up and observed signals on a multi-channel oscilloscope

15.8.1. *Electronic equipment*

Figure 15.16 shows the electronic equipment required. The following apparatus are necessary:

– generator, wobulator and synthesizer. Utilization of a quartz piloted generator is necessary to obtain greater accuracy. Eventually, a one current generator is used with a wobulator (to observe the presence of resonances across a frequency range) and a special quartz piloted generator;

– wide band amplifiers. The power required to excite all the emitter-transducers is not high; 10 to 50 watts is sufficient. It is necessary to have two power amplifiers so as to obtain two electric signals of opposite phase, or in phase. This couple of amplifiers permits both symmetric and anti-symmetric vibration motions to be obtained, as presented above;

– a phase inverter to obtain two signals equal in amplitude and opposite in phase so as to obtain symmetric and anti-symmetric displacements according to the kind of waves one wants to obtain (extensional, bending, or torsional);

– a frequency meter, where a quartz piloted generator is not available;

– two (or more) multi-channel oscilloscopes to observe the emitted and received signals at both ends of the rods.

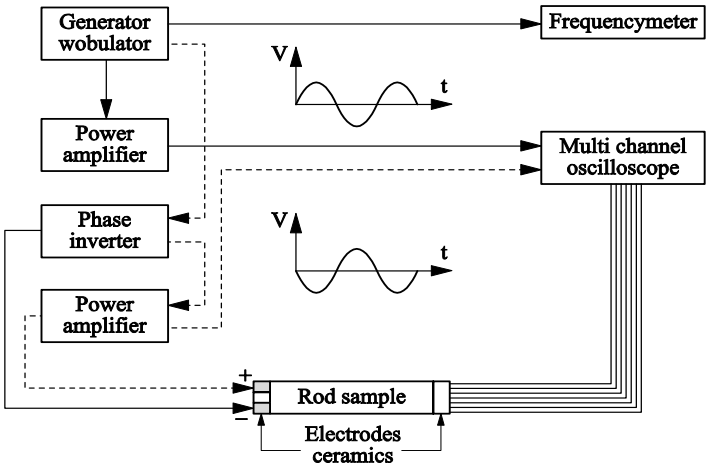

Figure 15.16. *Electronic equipment required to visualize the three types of motion and various elastodynamic modes*

15.8.2. *Signals representing various motions in rods*

When installing transducers, we will have already chosen the type of waves we desire to observe. Longitudinal, torsional or bending waves are created separately and analyzed, giving rise to transducers which are different in their polarizing vector $\vec{D}$ and in the nature of the symmetry of the wave itself, as presented above. However, it is inevitable that experimenters deal with parasitic signals due to defects in mounting and installing the transducers themselves.

15.8.2.1. *Longitudinal (extensional) stationary waves*

Figure 15.17(a) shows the first elastodynamic modes. The first mode corresponds to the receiver array of transducers which delivers signals of the same phase. The working frequency is indicated in the figure. Figure 15.17(b) corresponds to the second elastodynamic mode. Signals are delivered by two extreme receiver transducers in opposite phase. Figure 15.17(c) shows the third elastodynamic modes for five array transducer signals of opposite phase, for two neighboring transducers.

15.8.2.2. *The two first elastodynamic bending modes*

Figure 15.18 shows the two first modes. Figure 15.18(a) shows that all the vibration signals delivered by the array are in phase. Figure 15.19(b) shows three groups of signals which are in opposite phase. Remember that bending motion is symmetrical in nature and signals furnished by transducers at the peripherals must be in phase.

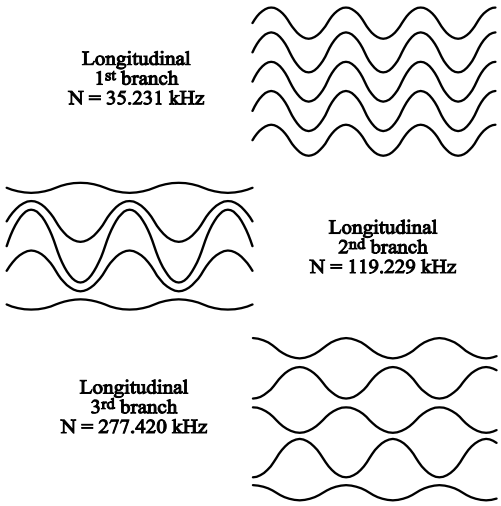

Figure 15.17. *The three first elastodynamic extensional modes visualized. Material: steel. The working frequency is greatly extended in the ultrasonic range*

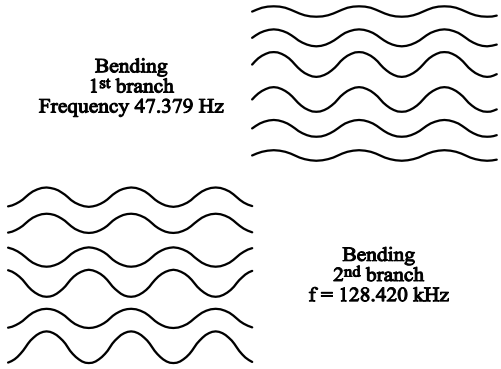

Figure 15.18. *Visualization of bending motion for various elastodynamic modes: (a) first modes; (b) second modes*

Remember that the disposition (number of transducers in the receiver array) and the relative phase of signals delivered by neighboring transducers in the array must be taken into account. Figure 15.19 shows four groups of transducers for the three first elastodynamic modes; for the first mode there is only one change of phase for the two groups of transducers. Remember also that the number of transducers in the array must be really even with respect to the anti-symmetric nature of this kind of wave.

15.8.2.3. *The three first elastodynamic torsional modes*

Figure 15.19(b) shows four changes of phase for the second mode and Figure 15.19(c) shows six changes of phase for the third mode.

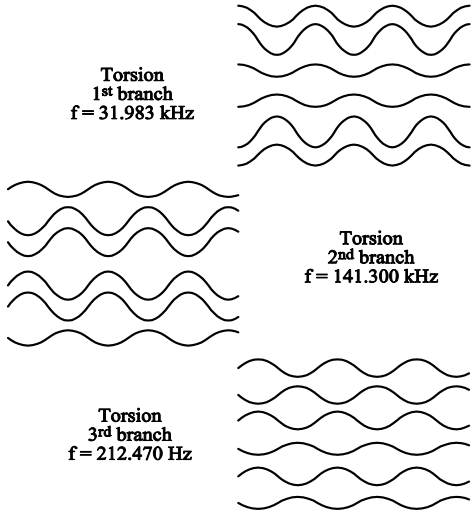

Figure 15.19. *Visualization of three torsional (shear) elastodynamic modes. Material: steel The so-called branch rank is related to the elastodynamic mode which are distinguished from one another by the odd number of phase changes – one in first mode, upper figure; three phase changes for second mode, middle figure; and five phase change for the third elastodynamic mode*

15.9. Presentation of experimental results

15.9.1. *Frequency spectrum of the two first elastodynamic modes for three types of waves*

Measurements were effected on two steel rods whose dimensions were 0.500×0.008× 0.020 m^3 and 1.000×0.020×0.040 m^3 (length×thickness×width). The number of resonance frequency varies with the elastodynamic mode rank and also with the rod length. In the curves presented below, reduced circular frequency is used, such that $\bar{\omega} = \frac{a_1 \omega}{c_0}$ where $\omega = 2\pi N$, a_1 is half of the rod thickness, and c_0 the velocity of the longitudinal wave at very low frequency, where $c_0 = \sqrt{\frac{E}{\rho}}$.

The reduced wave number is: $\bar{k} = ka_1 = 2\pi a_1 / \Lambda$; where Λ is the wavelength.

15.9.2. *Six first experimental elastodynamic modes of extensional waves*

Figure 15.20 shows six experimental elastodynamic modes compared to theoretical curves obtained by Touratier [TOU 79] using Reissner-Hellinger's variational principle with a displacement field of order three. Satisfactory agreement is obtained for elastodynamic modes up to the fourth mode. Discrepancies occur for the fifth and sixth modes. This is due to the displacement field being reduced to order three.

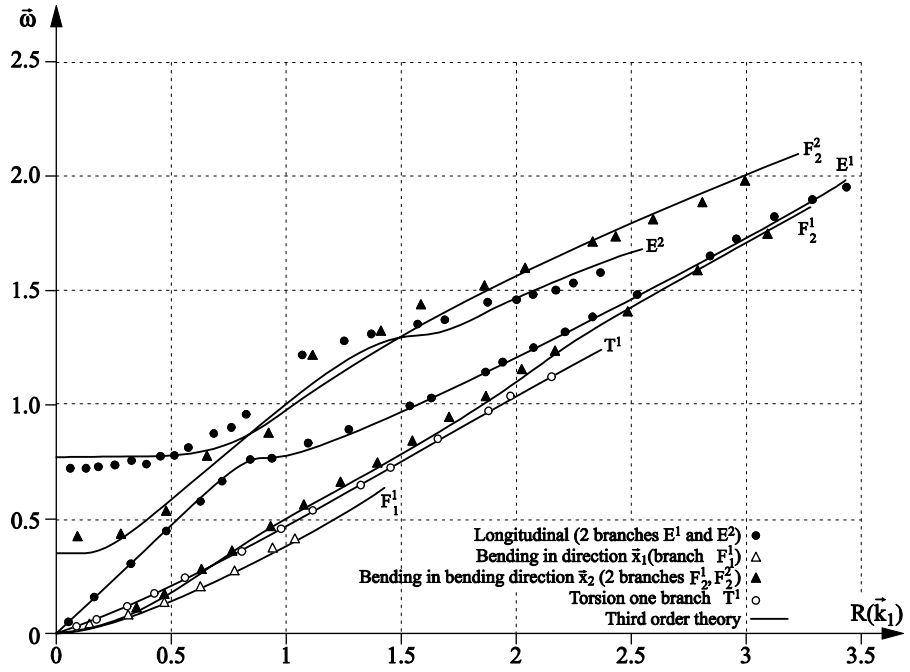

Figure 15.20. *Experimental frequency spectrum of a steel rod with a rectangular cross-section. Experimental points: • longitudinal waves with two branches (elastodynamic modes) E^1 and E^2 the two upper curves. The continuous line concerns theory and points, experimental curves; Δ bending wave in the direction $\overrightarrow{x_1}$ with one branch F_1^1; ▲: bending direction $\overrightarrow{x_2}$ with two branches F_2^1 and F_2^2; o torsion, one branch T^1*

15.9.3. *Six first experimental elastodynamic bending modes of a steel rod*

A third order theory is adopted in Hellinger-Reissner's theory by Touratier. For the three first elastodynamic modes, agreement of theoretical problem formulation and experimental studies are satisfactory. For the three higher elastodynamic modes, there are discrepancies due to the restricted number of terms retained in the series expansion.

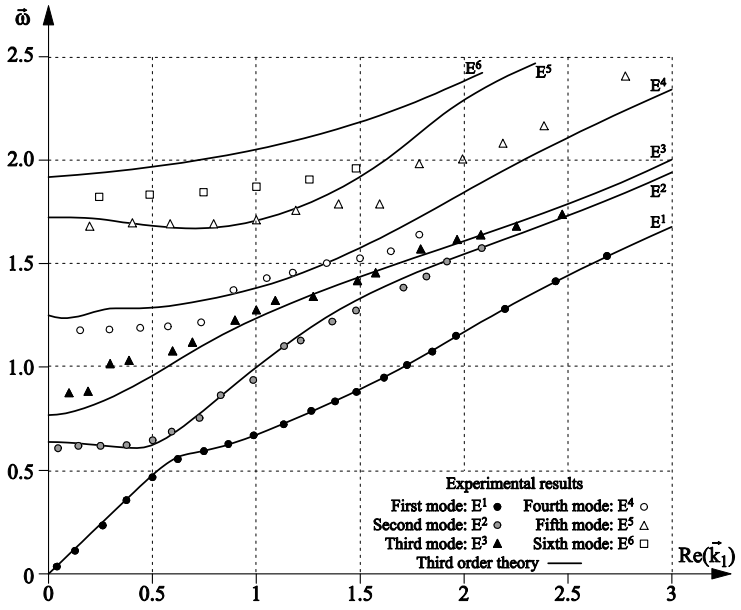

Figure 15.21. *Extensional waves: three elastodynamic modes obtained from experimental results. First mode E^1, second mode E^2, third mode E^3, fourth mode E^4, fifth mode E^5, sixth mode E^6*

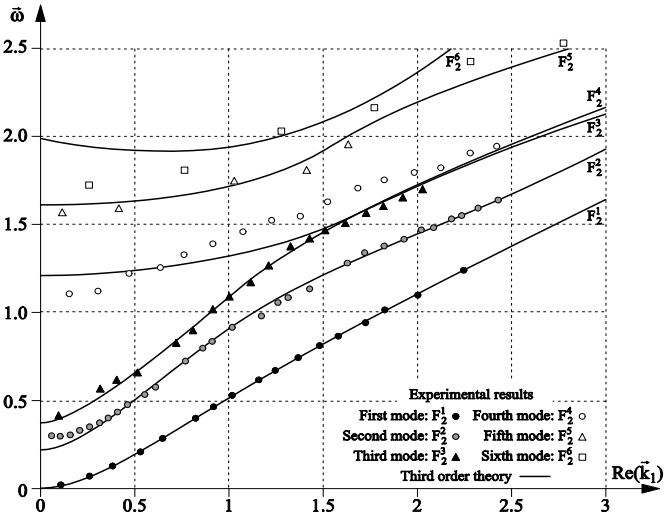

Figure 15.22. *Confrontation theory experiments. Bending waves at various elastodynamic modes. Superscripts designate the mode order. Bending is in the direction* $\overrightarrow{x_2}$

15.9.4. *Six first elastodynamic modes in torsion of a steel rod*

The confrontation between theory and experiments shows that using a theory with order three (field of displacement reduced to three terms in series expansion) shows that agreement is satisfactory up to the order five for elastodynamic modes, contrary to the two other kinds of waves presented above. Figure 15.22 shows experimental results against the theoretical formulation obtained by Touratier.

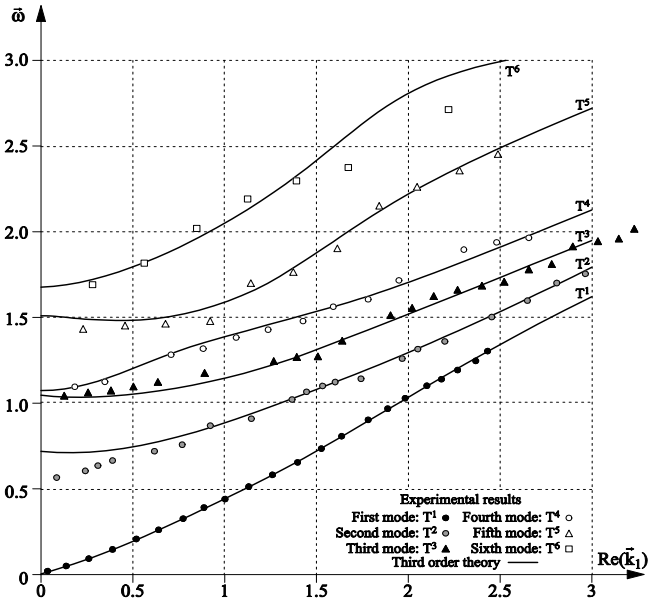

Figure 15.23.*Experimental frequency spectrum of torsional motion. for a teel rod with flatness e= 0.4. • First mode T^1, ○ Second mode T^2, ▲ Third mode T^3, o Fourth mode T^4, Δ Fifth mode T^5, □ Sixth mode (continuous line: third order Touratier's theory)*

15.10. Concluding remarks

This chapter has two levels of objectives. The following items outline the main points:

a) the theoretical formulation of the rod vibration problem. The literature is very prolific on this aspect. For an experimenter tackling the wave dispersion problem for the first time, it seems difficult to adopt a correct theory to cover a frequency range, particularly for extensional waves;

b) boundary conditions need to be satisfied. The main idea to retain is that theoretical formulation of vibration problems using a simple field of displacement, even when one adopts series expansion with a profusion of terms (up to 12 terms)

does not necessarily satisfy all the boundary conditions. This insurmountable difficulty is the reason for the weakness of some theories in the study of dispersion problems, particularly in the higher frequency range;

c) mixed fields of displacement and stress. In some cases, it is not necessary to appeal to complicated fields of displacement when using Hellinger–Reissner's variational principle. A mixed field with a reduced number of terms for the displacement series and for stress components is more efficient than using a sophisticated simple displacement field with a greater number of terms for displacement components, when using Hamilton's principle;

d) experimental studies of dispersion curves. This chapter shows that it is not complicated to conceive and realize mechanical or electronic equipment, special transducers and arrays of transducers to go beyond the first elastodynamic mode. Higher modes, in this respect, are not necessarily confined to academic studies. Corresponding waves can be produced with simple ferroelectric materials and fabrication of special transducers for this objective are not out of the reach of experimenters.

e) useful aspects of wave dispersions. Wave dispersions are presented at length in many chapters and open a new field of experimentation for the vast problem of dynamic characterization of materials and also fracture dynamics.

15.11. Bibliography

[BAR 62] BARR A.D.S., "Torsional waves in uniform rods of non circular section", *Journal of Mechanical Sciences*, Vol. 4, no. 2, 1962.

[CHE 75] CHEVALIER YVON, *Various Methods of Previsional Calculus for Composite Materials*, Sciences et technique de l'Armement, Third fascicule, 1975.

[CHE 10] CHEVALIER Y., VINH J. T. (ED.), *Mechanics of Viscoelastic Materials and Wave Dispersions,* ISTE Ltd, London and John Wiley & Sons, New York, 2010.

[FRA 69] FRASER .B., "Stress wave propagation in rectangular bars", *Int. Journal of Solid and Structures*, Vol.5, pp.379–397, 1969.

[MED 68] MEDICK M.A., "Extensional waves in elastic bars of rectangular cross section", *Journal Acoustical Soc. Amer.,* Vol. 43, no.1, p.152, 1968.

[MIN 60] MINDLIN R.D., FOX E.A., "Vibrations and waves in elastic bars of rectangular cross section", *Journal of Applied Mechanics*, Transactions of ASME, Series E, volume 27, pp.152–158, 1960.

[NIG 68] NIGRO N.J., "Wave propagation in anisotropic bars of rectangular cross section, Part I , Longitudinal wave propagation", *J. Acout. Soc. Americ.*, vol. 43, no. 5, 1968.

[TIM 21] TIMOSHENKO S.P., "On the correction for shear of the differential equation for transverse vibrations of prismatic bars", *Phil. Mag*., Series 6, 41, p.744, 1921.

[TOU 77] TOURATIER M., On the Propagation of Longitudinal Waves on Rectangular Composite Rods, Dissertation, CNAM, Paris, in French, 1977.

[TOU 79] TOURATIER M., On the Propagation of Waves in Transverse Isotropic Rod with Rectangular Cross Section. Thesis dissertation, University of Pierre and Marie Curie Paris, in French, May 30, 1979.

[VOL 61] VOLTERRA E., "Second approximation of method of internal constraints and its application", *International Journal of Mechanical sciences*, Pergamon Press, Vol. 3, pp.47–67, 1961.

[WAD 73] WADE J.E., TORVIK P.J., "Elastic wave propagation in homogeneous bars of several sections", *Journ. of Applied Mechanics*, ASME, p. 1050, December 1973.

15.12. Appendix 15A. Touratier's theory using Hellinger–Reissner's mixed fields

The variational Hamilton's principle with one displacement field was often used to study extensional motion coupled with transverse and shear motion. However, unfortunately, all the boundary conditions were not satisfied for stress components.

The mixed field Hellinger–Reissner's principle enables the displacement field and stress field to be adopted separately. All the boundary conditions are satisfied. This constitutes the main advantage of this variational formulation.

15A.1. *Outline of Touratier's mixed field theory*

15A.1.1. *General hypotheses*

a) Nature and symmetry of the material. The material is supposed to be homogenous and has an isotropic plane normal to axis $O\overrightarrow{x_3}$. This axis is a geometrical symmetry axis of the rod.

b) Test functions. All the test functions belong to the class C^m and the series adopted for displacement u_j and for stress σ_{ij} are convergent.

c) Free surface boundaries. The lateral surfaces of the rod are free of any stress components.

15A.1.2. *Construction of displacement field and stress field*

15A.1.2.1. Displacement field

The displacement field is represented by the following series:

$$\vec{u}(M,t) = \sum_{i=1}^{3} u_i(M,t)\,\vec{x}_i \qquad [15.A.1]$$

with $M_0 = (0,0,x_3)$.

[15.A.1] is written as follows:

$$u_i(M,t) = u_i^{00}(x_3,t) + x_1 u_i^{10}(x_3,t) + x_2 u_i^{01}(x_3,t) \qquad [15.A.2]$$

This is a one-dimensional formulation of displacement.

15A.1.2.2. Stress field

Stress components must satisfy the following conditions:

C_1: They are set to zero on lateral boundaries of the rod.

C_2: In a cross-section of the rod, a distribution of stress components is similar to that of displacement and satisfying the constitutive equation:

$$\sigma_{ij} = C_{ijkl}\,\varepsilon_{kl}$$

C_3: All the stress component distributions are relatively easy to manipulate in energy calculations. The first condition C_1 gives rise to vectorial equality:

$$\left.\begin{array}{l} \vec{T}(P,n] = \vec{0} \\ \forall\, P \in \partial D_L \end{array}\right\} \qquad [15.A.3]$$

where $\vec{T}$ is the stress vector, P is a point on the free boundary ∂D_L, $\vec{n}$ external normal to ∂D_L. The cross-section is defined as $[2a_1, 2a_2]$.

The following scalar equations are deduced:

$$(\sigma_{ii}) \equiv 0\ ,\ i = 1,2;\ x_i = \pm a_i \qquad [15.A.4]$$

$$(\sigma_{ij}) \equiv 0,\ j = 2,3;\ x_1 = \pm a_1 \qquad [15.A.5]$$

$$(\sigma_{ij}) \equiv 0,\ j = 3,1;\ x_1 = \pm a_2 \qquad [15.A.6]$$

With variable change:

$$\xi_i = x_i/a_i \ , \quad i = 1,2 \qquad [15.A.7]$$

Equalities [15.A.4] to [15.A.6] are satisfied with functions which are zero for $|\xi_i|=1$. Among elementary functions, cosine function: $\cos\frac{\pi}{2}\xi_I$ has this property and is not zero for $\xi_i = 0$, as the function $\sin\frac{\pi}{2}\xi_i$ takes the values identical to linear function for $|\xi_i|=1$ and $\xi_i=0$.

The utilization of such trigonometric functions seems to be appropriate.

15A.1.2.3. Expression of [15.A.2]

$$u_i(M,t) = \sum_{p=0}^{\infty} \sum_{q=0}^{\infty} \sin^p \frac{\pi\xi_1}{2}.\sin^q \frac{\pi\xi_2}{2} u_i^{pq}(x_3,t) \qquad [15.A.8]$$

$i \in \{1,2,3\}$; $(p,q) \in N$

15A.1.2.4. Expression of $\sigma_{ij}(M,t)$

Taking [15.A.4] and [15.A.6] into account:

$$\sigma_{ij}(M,t) = \sum_{p=0}^{\infty} \sum_{q=0}^{\infty} \left[\sin^p \frac{\pi\xi_1}{2}.\alpha_i(\xi_1).\sin^q \frac{\pi\xi_2}{2}.\beta_j(\xi_2) \right] \sigma_{ij}^{pq}(x_3,t) \qquad [15A.9a]$$

In [15.A.9a] two new coefficients are introduced

$$\alpha_i(\xi_1) = \cos\frac{\pi}{2}\xi_1, \ (i=1, j=1,2,3) \ , \ \alpha_i(\xi_1)=1 \ \ \forall i \neq 1$$

$$\beta_j(\xi_2) = \cos\frac{\pi}{2}\xi_2, \quad (i=2, j=2, 3), \ i=1, j=2$$

$$\text{if not } \beta_j(\xi_2) \equiv 1 \qquad [15.A.9b]$$

Note: the fields $\vec{u}$ and $\overline{\vec{\sigma}}$ are independent. [15.A.9a] and [15.A.9b] are not deduced from [15.A.8] by a classical elastic constitutive equation. However, conditions C_1 and C_2 are satisfied, i.e. there are free lateral boundaries and distribution of stress components similar to MacLaurin's series expansion of a stress vector. In [15.A.8] expansion of functions of ξ_1 and ξ_2 allows [15.A.1] to be found again by using substitution of functions.

15A.2. *General equations deduced from the two fields principle*

The Hellinger–Reissner principle is represented by the following integral action.

$$J(\vec{u}, \sigma) = \iiint_D (\rho \dot{u}_\iota \dot{u}_\iota + u_i \sigma_{ij,j} - u_{i,j}\sigma_{ij} + \sigma_{kl} S_{klij}\, \sigma_{ij} + 2u_i f_i)\, dV$$

$$-\iint_{\partial D_F} u_i\,(\sigma_{ij} n_j - 2F_i) dS_F + \iint_{\partial D_u} (u_i - 2\widehat{u_i})\, \sigma_{ij} n_j\, dS_u \qquad [15.A.10]$$

which can be formally written as:

$$J(\vec{u}, \sigma) = J_1 + J_2 - J_3 + J_4 + J_5 - J_6 + J_7 \qquad [15.A.11]$$

The seven integrals come from seven terms in [15.A.10]. The stationarity of this functional, in the time interval (t_1, t_2), is ensured by the two fields $\vec{u}$ and $\vec{\sigma}$ if:

$$\delta \int_{t_1}^{t_2} J(\overrightarrow{u}, \sigma)\, dt = 0 \; ; \quad \forall \delta u_i^{mn}; \forall \delta \sigma_{ij}^{pq} \qquad [15.A.12]$$

The domain D is defined as

$$D = [-a_1, a_1] \times [-a_2, a_2] \times [0, L]$$

By adopting dimensionless variables, domain D becomes $\widetilde{D}$ such as

$$\widetilde{D} = [-1,1] \times [-1,1] \times [0,1]$$

Extremely lengthy calculations were presented in Touratier's thesis [TOU 79]. We present the guidelines here.

15A.3. *Formulation of the boundary condition problem*

The seven integrals in [15.A.11] are evaluated. The three stress conditions indicated in [15.A.4, 15.A.5 and 15.A.6] are each examined.

15A.3.1. *First case: force prescribed at the rod ends $x_3=0$ and $x_3 = L$*

$$\left.\begin{aligned} -\sum_{r,s\geq 0} \alpha_{mnrs}^i\, \sigma_{i3}^{rs}(L,t) + \iint_{\partial D_F} F_i(\xi_1,\xi_2,L,t)\, \sin^m \frac{\pi}{2}\xi_1 .\, \sin^n \frac{\pi}{2}\xi_2\, d\xi_1\, d\xi_2 = 0 \\ \sum_{r,s\geq 0} \alpha_{mnrs}^i\, \sigma_{i3}^{rs}(0,t) + \iint_{\partial D_F} F_i(\xi_1,\xi_2,0,t) \sin^m \frac{\pi}{2}\xi_1 . \sin^n \frac{\pi}{2}\xi_2 .\, d\xi_1 d\xi_2 = 0 \end{aligned}\right\} \qquad [15.A.13]$$

(with $i \in \{1,2,3\}$).

$$\alpha^1_{mnrs} = d_{m+r,1}b_{n+s}\ ,\quad \alpha^2_{mnrs} = b_{m+r}d_{n+s,1}\ ,\quad \alpha^3_{mnrs} = b_{m+r}b_{n+s} \qquad [15.A.14]$$

Coefficients in [15.A.14] serving to evaluate [15.A.13] are used to express equations [15.A.13] under close form expressions.

15A.3.2. *Second case: displacements $\hat{u}_i$ imposed on the ends $x_3 = 0$ and $x_3 = L$*

$$\sum_{r,s\geq 0} \alpha^i_{mnrs}\, u_i^{rs}(L,t) - \iint_{\partial D_u} \hat{u}_i(\xi_1,\xi_2,L,t)\, \sin^m \frac{\pi}{2}\xi_1\, \sin^n \frac{\pi}{2}\xi_2 .\, \cos\frac{\pi}{2}\xi_i d\xi_1 d\xi_2 = 0$$

$$-\sum_{r,s\geq 0} \alpha^i_{mnrs}\, u_i^{rs}(0,t) + \iint_{\partial D_u} \hat{u}_i(\xi_1,\xi_2,0,t)\, \sin^m\frac{\pi}{2}\xi_1 \sin^n\frac{\pi}{2}\xi_2 \cos\frac{\pi}{2}\xi_i\, d\xi_1 d\xi_2 = 0 \qquad [15.A.15]$$

$i \in \{1,2,3\}$; $\cos\frac{\pi}{2}\xi_i = 1$ if $i=3$

15A.3.3. *Third case: mixed conditions: prescribed displacements at $x_3 = 0$ and prescribed at $x_3 = L$*

$$-\sum_{r,s\geq 0} \alpha^i_{mnrs}\, u_i^{rs}(0,t) + \iint_{\partial D_u} \hat{u}_i(\xi_1,\xi_2,0,t) \sin^m \frac{\pi}{2}\xi_1 \sin^n \frac{\pi}{2}\xi_2 \cos\frac{\pi}{2}\xi_i d\xi_1 d\xi_2 = 0$$

$$\sum_{r,s\geq 0} \alpha^i_{mnrs}\, \sigma_{i3}^{rs}(L,t) + \iint_{\partial D_u} F_i(\xi_1,\xi_2,L,t)\, \sin^m\frac{\pi}{2}\xi_1 \sin^n\frac{\pi}{2}\xi_2 d\xi_1 d\xi_2 = 0 \qquad [15.A.16]$$

15A.4. *Symmetry considerations concerning the three kinds of motion*

15A.4.1. *Extensional motion*

The following remarks will serve to us to express displacement and stress fields:

– the displacement components u_1 u_2 are anti-symmetric functions of x_1 and x_2 and symmetric with respect to x_2 and x1, respectively;

– axial displacement u_3 is a symmetric function of x_1 and x_2.

The displacement field is:

$$\left.\begin{aligned} u_1 &= \sum_{i,j\geq 0} \sin^{2i+1}\frac{\pi}{2}\xi_1 \sin^{2j}\frac{\pi}{2}\xi_2\, u_1^{2i+1,2j}(x_3,t) \\ u_2 &= \sum_{i,j\geq 0} \sin^{2i}\frac{\pi}{2}\xi_1 \sin^{2j+1}\frac{\pi}{2}\xi_2\, u_2^{2i,2j+1}(x_3,t) \\ u_3 &= \sum_{i,j\geq 0} \sin^{2i}\frac{\pi}{2}\xi_1 \sin^{2j}\frac{\pi}{2}\xi_2\, u_3^{2i,2j}(x_3,t) \end{aligned}\right\} \qquad [15.A.17a]$$

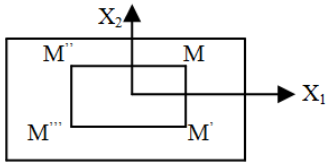

$(u_1, u_2, u_3)_M$
$(-u_1, u_2, u_3)_{M'}$
$(u_1, -u_2, u_3)_{M''}$
$(-u_1, -u_2, u_3)_{M'''}$

Figure 15A.1. *The four points M, M', M'', M''' give rise to displacement components indicated above*

15A.4.1.2. *The stress field*

$$\sigma_{11}= \sum_{i,j\geq 0} \sin^{2i}\frac{\pi}{2}\xi_1 .\cos\frac{\pi}{2}\xi_1 .\sin^{2j}\frac{\pi}{2}\xi_2.\sigma_{11}^{2i,2j}(x_3,t)$$

$$\sigma_{22} = \sum_{i,j\geq 0} \sin^{2i}\frac{\pi}{2}\xi_1 .\sin^{2j}\frac{\pi}{2}\xi_2 .\cos\frac{\pi}{2}\xi_2.\sigma_{22}^{2i,2j}(x_3, t)$$

$$\sigma_{33} = \sum_{i,j\geq 0} \sin^{2i}\frac{\pi}{2}\xi_1 .\sin^{2j}\frac{\pi}{2}\xi_2.\ \sigma_{33}^{2i,2j}(x_3,t)$$

$$\sigma_{23}= \sum_{i,j\geq 0} \sin^{2i}\frac{\pi}{2}\xi_1 .\sin^{2j+1}\frac{\pi}{2}\xi_2.\cos\frac{\pi}{2}\xi_2.\sigma_{23}^{2i,2j+1}(x_3,t)$$

$$\sigma_{31}= \sum_{i,j\geq 0} \sin^{2i+1}\frac{\pi}{2}\xi_1 .\cos\frac{\pi}{2}\xi_1.\sin^{2j}\frac{\pi}{2}\xi_2 .\sigma_{31}^{2i+1,\,2j}(x_3,t)$$

$$\sigma_{12} =\sum_{i,j\geq 0} \sin^{2i+1}\frac{\pi}{2}\xi_1.\cos\frac{\pi}{2}\xi_1.\sin^{2j+1}\frac{\pi}{2}\xi_2.\sigma_{12}^{2i+1,\,2j+1}(x_3,t)$$

[15.A.17b]

The next step is to write constitutive equations of materials relating the stress components in [15.A.17b] to the displacement components in [15.A.17a]. Derivatives of displacement components with respect to coordinates give rise to a number of intermediate coefficients [TOU 79].

The last step is to write down boundary conditions for the extensional symmetrical motion.

15A.4.2. *Bending motion*

Bending motion in the direction $\overrightarrow{x_2}$ gives rise to the following displacement components: the lateral component u_1 is an anti-symmetric function of x_1,x_2. Lateral component u_2 is a symmetric function of x_1 and x_2.

The longitudinal component u_3 is a symmetric function of $x_1$and an anti-symmetric function of x_2.

$$u_1 = \sum_{i,j\geq 0} \sin^{2i+1}\frac{\pi}{2}\xi_1 .\sin^{2j+1}\frac{\pi}{2}\xi_2 .u_1{}^{2i+1,2j+1}(x_3,t)$$

$$u_2 = \sum_{i,j\geq 0} \sin^{2i}\frac{\pi}{2}\xi_1 .\sin^{2j}\frac{\pi}{2}\xi_2 . u_2{}^{2i,2j}(x_3,t) \qquad [15.A.18a]$$

$$u_3 = \sum_{i,j\geq 0} \sin^{2i}\frac{\pi}{2}\xi_1 .\sin^{2j+1}\frac{\pi}{2}\xi_2 .u_3{}^{2i,2j+1}(x_3,t)$$

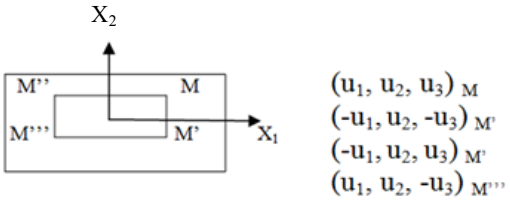

Figure 15A.2. *The four points M, M', M'' , M''' in the cross-section with the corresponding displacement components*

The stress field is as follows:

$$\sigma_{11} = \sum_{i,j\geq 0} \sin^{2i}\frac{\pi}{2}\xi_1 .\cos\frac{\pi}{2}\xi_1 .\sin^{2j+1}\frac{\pi}{2}\xi_2 . \sigma_{11}{}^{2i,2j+1}(x_3,t)$$

$$\sigma_{22} = \sum_{i,j\geq 0} \sin^{2i}\frac{\pi}{2}\xi_1 .\sin^{2j+1}\frac{\pi}{2}\xi_2 .\cos\frac{\pi}{2}\xi_2 . \sigma_{22}{}^{2i,2j+1}(x_3,t)$$

$$\sigma_{33} = \sum_{i,j\geq 0} \sin^{2i}\frac{\pi}{2}\xi_1 .\sin^{2j+1}\frac{\pi}{2}\xi_2 .\sigma_{33}{}^{2i,2j+1}(x_3,t)$$

$$\sigma_{23} = \sum_{i,j\geq 0} \sin^{2i}\frac{\pi}{2}\xi_1 .\sin^{2j}\frac{\pi}{2}\xi_2 .\cos\frac{\pi}{2}\xi_2 .\sigma^{2i,2j}{}_{23}(x_3,t) \qquad [15.A.18b]$$

$$\sigma_{31} = \sum_{i,j\geq 0} \sin^{2i+1}\frac{\pi}{2}\xi_1 .\cos\frac{\pi}{2}\xi_1 .\sin^{2j+1}\frac{\pi}{2}\xi_2 .\sigma_{31}{}^{2i+1,2j+1}(x_3,t)$$

$$\sigma_{12} = \sum_{i,j\geq 0} \sin^{2i+1}\frac{\pi}{2}\xi_1 .\cos\frac{\pi}{2}\xi_1 .\sin^{2j}\frac{\pi}{2}\xi_2 .\cos\frac{\pi}{2}\xi_2 . \sigma_{12}{}^{2i+1,2j}(x_3,t)$$

15A.4.3. *Symmetric shear (torsional) motion*

This motion is effected around longitudinal axis $\overrightarrow{0x_3}$. It is characterized by the three following displacement components:

– the radial components u_1 is symmetric function of x_1 and antisymetric function of x_2, u_2 is antisymmetric functions of x_1 and symmetric function of x_2 ;

– longitudinal component u_3 along axis $0\overrightarrow{x_3}$ is an anti-symmetric function of the two lateral coordinates x_1, x_2.

The dissymmetry of the longitudinal components is related to section warping.

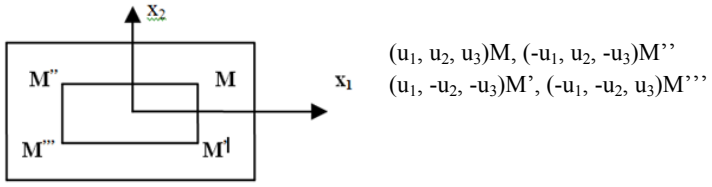

Figure 15A.3. *Displacement components of four points in the cross-section in torsion motion: M, M', M'', M'''*

$$\left.\begin{aligned} u_1 &= \sum_{i,j\geq 0} \left(\sin^{2i}\frac{\pi}{2}\xi_1.\sin^{2j+1}\frac{\pi}{2}\xi_2\right).\ u_1{}^{2i,\,2j+1}(x_3,t) \\ u_2 &= \sum_{i,j\geq 0} \left(\sin^{2i+1}\frac{\pi}{2}\xi_1\sin^{2j}\ \frac{\pi}{2}\xi_2\right) u_2{}^{2i+1,2j}\,(x_3,t) \\ u_3 &= \sum_{i,j\geq 0} \left(\sin^{2i+1}\frac{\pi}{2}\xi_1\sin^{2j+1}\frac{\pi}{2}\xi_2\right) u_3{}^{2i+1,2j+1}(x_3,t) \end{aligned}\right\} \quad [15.A.19a]$$

Components of stress are:

$$\left.\begin{aligned} \sigma_{11} &= \sum_{i,j\geq 0} \sin^{2i+1}\frac{\pi}{2}\xi_1.\cos\frac{\pi}{2}\xi_1\sin^{2j+1}\frac{\pi}{2}\xi_2.\sigma_{11}{}^{2i+1;2j+1}\,(x_3,t) \\ \sigma_{22} &= \sum_{i,j\geq 0} \sin^{2i+1}\frac{\pi}{2}\xi_1.\ \sin^{2j+1}\frac{\pi}{2}\xi_2.\cos\frac{\pi}{2}\xi_2\ .\ \sigma_{22}{}^{2i+1,2j+1}(x_3,\,t) \\ \sigma_{33} &= \sum_{i,j\leq 0} \sin^{2i+1}\frac{\pi}{2}\xi_1.\sin^{2j+1}\frac{\pi}{2}\xi_2.\sigma_{33}{}^{2i+1,2j+1}(x_3,t) \\ \sigma_{23} &= \sum_{i,j\geq 0} \sin^{2i+1}\frac{\pi}{2}\xi_1\ .\sin^{2j}\frac{\pi}{2}\xi_2.\cos\frac{\pi}{2}\xi_2.\sigma_{23}{}^{2i+1,2j}\,(x_3,t) \\ \sigma_{31} &= \sum_{i,j\geq 0} \sin^{2i}\frac{\pi}{2}\xi_1\ .\cos\frac{\pi}{2}\xi_1\ .\sin^{2j+1}\frac{\pi}{2}\xi_2.\sigma_{31}{}^{2i,2j+1}\,(x_3,t) \\ \sigma_{12} &= \sum_{i,j\geq 0} \sin^{2i}\frac{\pi}{2}\xi_1\ .\cos\frac{\pi}{2}\xi_1\ .\sin^{2j}\frac{\pi}{2}\xi_2\ .\cos\frac{\pi}{2}\xi_2.\sigma_{12}{}^{2i,2j}\,(x_3,t) \end{aligned}\right\} \quad [15.A.19b]$$

Equations of motion require the writing of constitutive equations of materials and also of boundary conditions.

In the three cases presented above, we do not present the six stress components which are written similarly to those used in [15.A.17, 15.A.18 and 15.A.19]. The coefficient of each stress component is, however, the product of three terms instead of two for displacement components.

15A.5. ***Truncating process for one dimensional theories: extensional waves***

Displacement components as well as stress components are represented by infinite series. It is not reasonable to keep these series as sums of infinite number of terms.

As a first step, we work to truncate these series. Let us begin with a first order truncation. This consists of retaining, in each series in [15.A.17] to [15.A.19], one term for each component of displacement and stress.

The second step consists of integrating using the functional $J(\vec{u},\sigma)$ bringing displacement components and stress components into [15.A.12].

The following displacement vector is obtained:

$$\vec{u}\,(M,t) = \sin\frac{\pi}{2}\xi_1.\, u_1^{10}.\overrightarrow{x_1} + \sin\frac{\pi}{2}\xi_2.u_2^{01}.\overrightarrow{x_2} + u_3^{00}.\overrightarrow{x_3} \qquad [15.20]$$

The stress components presented under matricial form are:

$$[\sigma] = \begin{pmatrix} \cos\frac{\pi\xi_1}{2}.\sigma_{11}^{00} & 0 & \frac{1}{2}\sin\frac{\pi\xi_1}{2}.\sigma_{31}^{10} \\ 0 & \cos\frac{\pi\xi_2}{2}.\sigma_{22}^{00} & \frac{1}{2}\sin\frac{\pi\xi_2}{2}.\sigma_{23}^{01} \\ \frac{1}{2}\sin\frac{\pi\xi_1}{2}.\sigma_{31}^{10} & \frac{1}{2}\sin\frac{\pi\xi_2}{2}.\sigma_{23}^{01} & \sigma_{33}^{00} \end{pmatrix} \qquad [15A.21]$$

The equations of motion are:

$$\left.\begin{array}{l} \rho\ddot{u}_1^{10} + \frac{\pi}{2a_1}\sigma_{11}^{00} - \frac{4}{3\pi}\sigma_{31,3}^{10} = 0 \\ \rho\ddot{u}_2^{01} + \frac{\pi}{2a_2}\sigma_{22}^{00} - \frac{4}{3\pi}\sigma_{23,3}^{01} = 0 \\ \rho\ddot{u}_3^{00} - \sigma_{33,3}^{00} = 0 \end{array}\right\} \qquad [15.A.22]$$

Constitutive equations are now introduced in [15.A.22] so as to eliminate stress components and retain only the displacement components and their time and space derivatives:

15A.6. *Equations of motion for extensional movement*

In the absence of volumic forces, we obtain the following equations:

$$\rho \ddot{u}_1^{10} = \frac{64}{9\pi^2 S_{44}} u_{1,33}^{10} + \frac{\pi^2}{4a_1^2\Delta_E}\left(8\frac{S_{13}^2}{\pi^2} - S_{11}S_{33}\right) u_1^{10} + \frac{2}{a_1\Delta_E}\left(S_{12}S_{35} - S_{13}^2\right) u_1^{01} + \frac{2S_{13}}{a_1\Delta_E}\left(S_{11} - 8\frac{S_{12}}{\pi^2}\right) u_{3,3}^{00} \quad [15.A.23a]$$

$$\rho \ddot{u}_2^{01} = \frac{64}{9\pi^2 S_{44}} u_{2,33}^{01} + \frac{\pi^2}{4a_2^2\Delta_E}\left(+\frac{8S_{13}^2}{\pi^2} - S_{11}S_{33}\right)u_2^{01} + \frac{2}{a_1 a_2\Delta_E}\left(S_{12}S_{33} - S_{13}^2\right) u_1^{10} + \frac{2S_{13}}{a_2\Delta_E}\left(S_{11} - \frac{8S_{12}}{\pi^2}\right)u_{3,3}^{00} \quad [15.A.23b]$$

$$\rho \ddot{u}_3^{00} = \frac{1}{\Delta_E}\left(S_{11}^2 - \frac{64S_{12}^2}{\pi^4}\right) u_{3,33}^{00} + \frac{S_{13}}{a_1\Delta_E}\left(\frac{8S_{12}}{\pi^2} - S_{11}\right) u_{1,3}^{00} + \frac{S_{13}}{a_2\Delta_E}\left(\frac{8S_{12}}{\pi^2} - S_{11}S_{13}\right) u_{2,3}^{01} \quad [15.A.23c]$$

$$\Delta_E = S_{11}\left(S_{11}S_{33} - \frac{8S_{13}^2}{\pi^2}\right) - \frac{64S_{12}}{\pi^4}\left(S_{12}S_{33} - S_{13}^2\right) + \frac{8S_{13}^2}{\pi^2}\left(\frac{8S_{12}}{\pi^2} - S_{11}\right) \quad [15.A.24]$$

where S_{ij} is the compliance matrix coefficient.

15A.6.1. *Physical interpretation of terms in equation [15.A.23]*

The terms $\ddot{u}^{10}_{1,33}$ and $\ddot{u}^{01}_{2,33}$ from the two first equations [15.A.23] describe the radial inertia for extensional motion.

Terms u_1^{10} and $u_{2,33}^{01}$ in the same equation represent lateral shear motion.

The other correction terms in [15.A.23] concern the intervention of the displacement field and stress field. They are consequently the terms describing vibration coupling.

The two last terms of the equation in [15.A.23] represent the equivalent, in elementary theory, to the coefficient of $u_{3;33}^{00}$:

$$\frac{1}{\Delta_E}\left(S_{11}^2 - \frac{64S_{12}^2}{\pi^2}\right)$$

which is different from the elementary theory term $\frac{1}{S_{33}}$.

15A.6.2. *Interpretation of vibration mode type by different displacement components in [15.A.2]*

The partial displacement component u_3^{00} corresponds to uniform translation (see Figure15A.4).

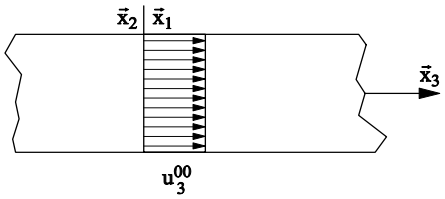

Figure 15A.4. *Fundamental longitudinal mode represented by displacement component u_3^{00} which is the only displacement component in elementary theory*

For partial displacement component u_1^{10} and u_2^{01}, longitudinal motion is accompanied by lateral contraction or expansion of the cross-section. This constitutes expansion modes in the thickness.

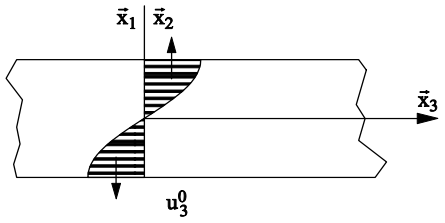

Figure 15A.5. *Lateral expansion and contraction modes associated with longitudinal modes*

15A.7. *Effective front velocity and wave front velocity*

These terms designate asymptotic values of velocities obtained from equations of motion at lower frequencies and at an upper frequency which tends to infinity.

Equations of motion (derived from [15.A.23]) are of the same order. They can be reduced to a unique equation of motion of the sixth degree:

$$-\frac{\partial^6 E}{\partial t^6} + e_1\frac{\partial^4 E}{\partial t^4} + e_2\frac{\partial^2 E}{\partial t^2} + e_3\frac{\partial^6 E}{\partial x_3^6} + e_4\frac{\partial^4 E}{\partial x_3^4} + e_5\frac{\partial^2 E}{\partial x_3^2} + e_6\frac{\partial^6}{\partial t^4\,\partial x_3^2} + e_7\frac{\partial^6 E}{\partial t^2\,\partial x_3^4} + e_8\frac{\partial^4 E}{\partial t^2\,\partial x_3^2} = 0 \qquad [15.A.25]$$

where E represents any displacement component among the trio of (u_1^{10}, u_2^{01}, u_3^{00}).

The progressive wave is obtained by writing:

$$E(x_3, t) = A.\exp j[kx-ct] \qquad [15.A.26]$$

where k is the wave number, and c the phase velocity. There are three phase velocities corresponding to three possible modes (types).

15A.7.1. *Wave front velocity*[8]

The upper bound limit C_{i00} of the three velocities is represented by the term of highest degree in [15,A.25] taking [15,A.26] into account:

$$c_\infty^6 = e_3 \qquad [15.A.27]$$

$$c_\infty^6 = \frac{1}{\overline{\Delta_E}}\left(\frac{64}{9\pi^2 S_{44}}\right)^2\left(S_{11}^2 - \frac{64S_{12}^2}{\pi^4}\right) \quad \text{where } s_{ij} = \frac{S_{ij}}{S_{33}} \quad \overline{\Delta_E} = \frac{\Delta_E}{S_{33}^2};\ \bar{c}^2 = \rho S_{33} c^2$$

So, when $k \to \infty$, the reduced phase velocity $\bar{c}_1$, $\bar{c}_2$, $\bar{c}_3$ for the first elastodynamic longitudinal modes are, respectively:

$$\overline{c_{1\infty}} = \overline{c_{2\infty}} = \frac{8}{3\pi\sqrt{s_{44}}} \qquad [15.A.28]$$

$$\overline{c_{3\infty}} = \left\{\frac{1}{\overline{\Delta_E}}\left(s_{11}^2 - \frac{64 s_{12}^2}{\pi^4}\right)\right\}^{1/2} \qquad [15.A.29]$$

Note: using [15,A.28] we obtain the relative velocity $\bar{c_1}$ which,is for isotropic elasticity:

$$\bar{c_1} \cong \frac{0{,}85}{\sqrt{s_{44}}}$$

Elementary theory gives $\overline{c_{1\infty}} = \frac{1}{\sqrt{s_{44}}} = \bar{c_T}$.

The difference between the two values can be explained by the fact that elementary theory cannot allow an asymptotic value of $\overline{c_T}$ to be obtained at an infinite frequency.

8 The velocity of each type of wave is related to components of displacement. At high frequency, the profile of a wave depends closely on the displacement components of a higher degree retained in the displacement series. The wave front profiles for the same type of wave (extensional, torsion, bending) are different from one theory to another.

Physically speaking, at a higher frequency, and in a homogenous material, waves tend to "concentrate" near the free surface and the velocity is given by Rayleigh's wave velocity. For an isotropic material, the Poisson's number is of the order 0.3 and Rayleigh's velocity approaches the value:

$$\overline{c_R} \cong 0.9\ \overline{c_T}$$

Touratier's theory gives:

$$\overline{c_{1\infty}} \cong 0.85\ \overline{c_T}$$

15A.7.2. *Effective wave front velocity*

The effective wave front is represented by the lowest degree in equation [15.A.25]. It corresponds to the wave number $k \to 0$

$$e_2 c_0^2 = -e_5$$

The corresponding reduced velocity is: $\overline{c_0}^2 = 1$.

This effective wave front propagates at the longitudinal wave velocity in the elementary theory. At higher frequency, c_0 cannot describe the behavior of an extensional wave. Higher degree terms in [15.A.25] have an influence which increases with frequency. These wave fronts (there are three waves) travel with imposed discontinuities, without damping.

15A.8. *Bending equations of motion*

Equation [15.A.18] proposes a displacement field for bending motion using a trigonometric double series for coefficients. For the first order approximation, truncation of the series is limited to the first term. Then the displacement vector is written as (i = 0,j = 0):

$$\vec{u}\ (M,t) = \sin\frac{\pi}{2}\xi_1.\sin\frac{\pi}{2}\xi_2.\ u_1^{11}\overrightarrow{x_1} + u_2^{00}\overrightarrow{x_2} + \sin\frac{\pi}{2}\xi_2.u_3^{01}\overrightarrow{x_3} \qquad [15.A.30]$$

The stress components are written in matricial form as:

$$[\sigma]=\begin{pmatrix} \cos\frac{\pi\xi_1}{2}.\sin\frac{\pi\xi_2}{2}\sigma_{11}^{00} & \frac{1}{2}\sin\frac{\pi\xi_1}{2}.\cos\frac{\pi\xi_2}{2}\sigma_{12}^{10} & \frac{1}{2}\sin\frac{\pi\xi_1}{2}.\sin\frac{\pi\xi_2}{2}\sigma_{31}^{11} \\ \frac{1}{2}\sin\frac{\pi\xi_1}{2}.\cos\frac{\pi\xi_2}{2}\sigma_{12}^{10} & \frac{1}{2}\sin\frac{\pi\xi_2}{2}.\sigma_{22}^{01} & \cos\frac{\pi\xi_2}{2}.\sigma_{23}^{00} \\ \frac{1}{2}\sin\frac{\pi\xi_1}{2}.\sin\frac{\pi\xi_2}{2}\sigma_{31}^{11} & \cos\frac{\pi\xi_2}{2}.\sigma_{23}^{00} & \sin\frac{\pi\xi_2}{2}\sigma_{33}^{01} \end{pmatrix} \quad [15.A.31]$$

The equations of motion are:

$$\left.\begin{array}{l} \rho\ddot{u}_1^{11}+\frac{\pi}{2a_1}\sigma_{11}^{01}+\frac{2}{3a_2}\sigma_{12}^{10}-\frac{4}{3\pi}\sigma_{31,3}^{11}=0 \\ \rho\,\ddot{u}_2^{00}-\frac{2}{\pi}\sigma_{23,3}^{01}=0 \\ \rho\,\ddot{u}_3^{01}+\frac{\pi}{2a_2}\sigma_{23}^{00}-\sigma_{33,3}^{01}=0 \end{array}\right\} \quad [15.A.32]$$

Constitutive equations of material permit 6 equations for six stress components to be obtained, and displacement components and their derivatives:

$$\left.\begin{array}{l} S_{11}\sigma_{11}^{01}+\frac{16}{3}\frac{S_{12}}{\pi^2}\sigma_{22}^{01}+\frac{4S_{13}}{\pi}\sigma_{33}^{01}=\frac{\pi}{2a_1}u_1^{11} \\ \frac{32}{3\pi^2}S_{12}.\sigma_{11}^{01}+S_{22}\sigma_{22}^{01}+\frac{16}{3\pi}S_{23}\sigma_{33}^{01}=0 \\ \frac{2S_{13}}{\pi}\sigma_{11}^{01}+\frac{4S_{23}}{3\pi}\sigma_{22}^{01}+S_{33}\sigma_{33}^{01}=u_{3,3}^{01} \\ S_{44}\sigma_{23}^{00}=\frac{4}{\pi}u_{2,3}^{00}+\frac{\pi}{2a_2}u_{1,3}^{11} \\ S_{44}.\sigma_{31}^{11}=\frac{16}{3\pi}u_{1,3}^{11} \\ S_{66}\sigma_{12}^{10}=\frac{8}{3a_2}u_1^{11} \end{array}\right\} \quad [15.A.33]$$

Note: if in [15.A.30] the first component is neglected:

$$\vec{u}(M,t)=u_2^{00}\overrightarrow{x_2}+\sin\frac{\pi}{2}\xi_2.\,u_3^{01}\overrightarrow{x_3}$$

$$\sigma_{33}=\sin\frac{\pi}{2}\xi 2\sigma_{33}^{01}\;;\quad \sigma_{23}=\cos\frac{\pi}{2}\xi 2.\sigma_{23}^{00}\;,$$

then [15.A.32] and [15.A.33] give the following equation:

$$\rho\ddot{u}^2_{00} + \frac{32}{\pi^4}\frac{a_2^2}{S_{33}} u^{00}_{2,33} = 0 \qquad [15.A.34]$$

This will be recognized as Bernoulli–Euler's equation. The ratio of the quadratic moment $I_1 = 4a_1a_2^3$ on the cross-section area gives:

$$I_1 / S = a_2^2 / 3 \cong 32a_2^2 / \pi^4$$

The coefficient $32/\pi^4$ is in [15A.34] as the second term.

15A.8.1. *Bending equations of motion*

Elimination of stress components permits the following set of equations of motion to be obtained:

$$\left.\begin{aligned}
\rho\, \ddot{u}_1{}^{11} &= \frac{64}{9\pi^2 S_{44}} u^{11}_{1,33} - \left\{ \frac{\pi^2}{4a_1^2\Delta_F}\left(S_{11}S_{33} - \frac{64S_{13}^2}{9\pi^2}\right) + \frac{16}{9a_2^2 S_{66}}\right\} u_1^{11} - \frac{2S_{13}}{a_1\Delta_F}\left(\frac{64S_{12}}{9\pi^2} - S_{11}\right) u^{01}_{3,3} \\
\rho\ddot{u}_2^{00} &= \frac{8}{\pi^2 S_{44}} u^{00}_{2,33} + \frac{1}{a_2 S_{44}} u^{01}_{3,3} \\
\rho\ddot{u}_3^{01} &= \frac{1}{\Delta_F}\left(S_{11}^2 - \frac{512S_{12}}{9\pi^4}\right) u^{01}_{3,33} + \frac{S_{13}}{a_1\Delta_F}\left(\frac{64S_{12}}{9\pi^2} - S_{11}\right) u^{11}_{1,3} - \frac{2}{a_2 S_{44}} u^{00}_{2,3} - \frac{\pi^2}{4a_2^2 S_{44}} u^{01}_3
\end{aligned}\right\} \qquad [15A.35]$$

where Δ_F is defined as:

$$\Delta_F = S_{11}\left(S_{11}S_{33} - \frac{64S_{13}^2}{9\pi^2}\right) - \frac{512S_{12}}{9\pi^4}\left(S_{12}S_{33} - S_{13}^2\right) + \frac{8}{\pi^2} S_{13}^2\left(\frac{64S_{12}}{9\pi^2} - S_{11}\right) \quad [15.A.36]$$

15A.8.2. *Physical interpretation of various displacement components*

1. The term $\ddot{u}_1^{11}$ constitutes a radial inertia correction.

2. The term $u^{11}_{1,33}$ concerns shear correction.

3. The other terms correspond to coupling terms.

4. Bending in direction $\overrightarrow{x_1}$ is deduced from the equations presented above by changing e into 1/e, the material being transversely isotropic.

15A.8.3. *Particle motion in bending vibration*

In Figure 15A.6 the mode associated with displacement component u_2^{00} is represented in Figure 15A.6(a) which corresponds to a uniform translation of the cross-section in the direction 0 $\overrightarrow{x_2}$. It is called the bending amplitude of the rod in the strength of material. This bending mode is coupled with two others modes, u_1^{11} and u_3^{01}, which are interpreted in Figure 15A.6(b).

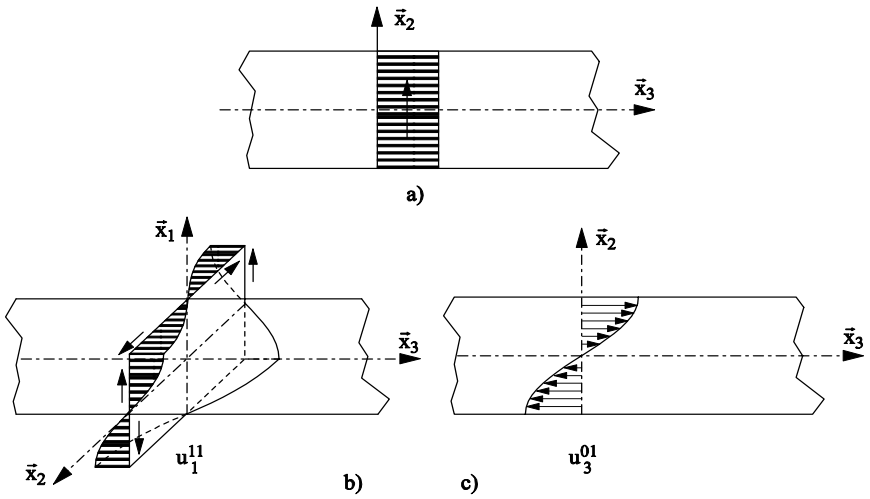

Figure 15A.6. *Bending motion: (a) motion of component u_2^{00};(b) motion of component u_1^{01}; (c) motion of component u_3^{01}*

15A.9. *Equations of motion: torsional vibration*

15A.9.1. *Equations of motion*

Truncating the series to the first order, we obtain the vector displacement:

$$\vec{u}(M,t) = \sin\frac{\pi}{2}\xi_2.u_{10}{}^1\overrightarrow{x_1} + \sin\frac{\pi}{2}\xi_1.u_{21}{}^0.\overrightarrow{x_2} + \sin\frac{\pi}{2}\xi_1.\sin\frac{\pi}{2}\xi_2.\ u_3{}^{11}.\overrightarrow{x_3} \qquad [15.A.37]$$

The stress field has following matricial representation:

$$[\sigma] = \begin{pmatrix} \frac{1}{2}\sin\pi\xi_1.\sin\frac{\pi}{2}\xi_2.\sigma_{11}{}^{11} & \cos\frac{\pi}{2}\xi_1\cos\frac{\pi}{2}\xi_2\ .\sigma_{12}{}^{00} & \cos\frac{\pi}{2}\xi_1\sin\frac{\pi}{2}\xi_2\sigma_{31}{}^{01} \\ \cos\frac{\pi}{2}\xi_1\cos\frac{\pi}{2}\boldsymbol{\xi_2}.\sigma_{12}{}^{00} & \frac{1}{2}\sin\frac{\pi}{2}\boldsymbol{\xi_1}\sin\pi\xi_2.\sigma_{22}{}^{11} & \sin\frac{\pi}{2}\xi_1\cos\frac{\pi}{2}\xi_2.\sigma_{23}{}^{10} \\ \cos\frac{\pi}{2}\xi_1.\sin\frac{\pi}{2}\xi_2.\sigma_{31}{}^{01} & \sin\frac{\pi}{2}\xi_1.\cos\frac{\pi}{2}\xi_2.\sigma_{23}{}^{10} & \sin\frac{\pi}{2}\xi_1\sin\frac{\pi}{2}\xi_2.\sigma_{33}{}^{11} \end{pmatrix} \qquad [15.A.38]$$

Equations of motion are obtained in a similar manner as for bending wave:

$$\left.\begin{aligned}
\rho\ddot{u}_1^{01} &= \frac{8}{\pi^2 S_{44}}u_{1,33}^{01} - \frac{2}{a_2^2 S_{66}}u_1^{01} - \frac{2}{a_1 a_2 S_{66}}u_{3,3}^{11} \\
\rho\ddot{u}_2^{10} &= \frac{8}{\pi^2 S_{44}}u_{2,33}^{10} - \frac{2}{a_1^2 S_{66}}u_2^{10} - \frac{2}{a_1 a_2 S_{66}}u_1^{01} + \frac{1}{a_2 S_{44}}u_{3,3}^{11} \\
\rho\ddot{u}_3^{11} &= \frac{1}{\Delta_T}\left\{S_{11}^2 - \left(\frac{64S_{12}}{9\pi^2}\right)^2\right\}u_{3,33}^{11} - \frac{\pi^2}{4S_{44}}\left(\frac{1}{a_1^2}+\frac{1}{a_2^2}\right) - \frac{2}{a_1 S_{44}}u_{1,3}^{01} - \frac{2}{a_2 S_{44}}u_{2,3}^{10}
\end{aligned}\right\} \quad [15.A.39]$$

Where

$$\Delta_T = \left(S_{11} - \frac{64S_{12}}{9\pi^2}\right)\left\{S_{33}\left(\frac{64S_{12}}{9\pi^2} + S_{11}\right) - \frac{128S_{13}^2}{9\pi^2}\right\} \quad [15.A.40]$$

Figure 15A.7 completes the mathematical formulation of the torsion problem in section 15A.4.3. The motion of axial component u_3^{11} in [15.A.6b] creates warping of the cross-section.

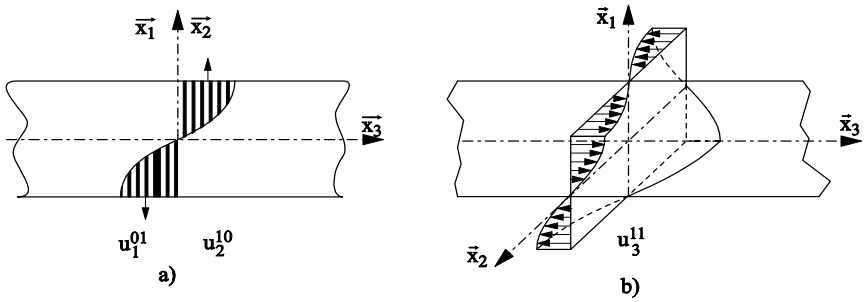

Figure 15A.7. *Torsional motion. (a) The two displacement components u_1^{01} and u_2^{10} are represented; (b) axial component u_3^{11} creates warping of the cross-section*

15.13. Appendix 15B. Third order Touratier's theory

The accuracy obtained for a given order of elastodynamic mode depends on the degree of decoupled equations of motion.

If this degree is 2n, the (n-1) first mode has good accuracy and the nth mode might have poor accuracy. The situation is similar to the problem of (eigenvalue) modes of a mechanical structure, which is governed by matricial equations with a matrix n×n. If calculations are effected with the Ritz's method, the n-1 first modes are acceptable whilst the last eigenvalue has poor accuracy.

This idea can be considered as a guide when truncating a set of series expressing displacement components and stress components.

In the framework of Reissner-Hellinger's variational principle, if we truncate each series to the third term, we obtain 9 branches for the frequency spectrum and we can be sure that the 8 first modes are correctly portrayed.

15B.1. *Extensional waves with nine evaluated modes*

From equation [15.A.17], three terms are retained for each series for displacement components, (i=0,j=0), (i=0,j=1), (i=1,j=0):

$$u_1 = \sin\frac{\pi\xi_1}{2}.u_1^{10} + \sin\frac{\pi\xi_1}{2}.\sin^2\frac{\pi\xi_2}{2}.u_1^{20} + \sin^3\frac{\pi\xi_1}{2}.u_1^{30}$$

$$u_2 = \sin\frac{\pi\xi_2}{2}.u_2^{01} + \sin\frac{\pi\xi_1}{2}.\sin\frac{\pi\xi_2}{2}.u_2^{21} + \sin^3\frac{\pi\xi_2}{2}.u_2^{03}$$

$$u_3 = u_3^{00} + \sin^2\frac{\pi\xi_1}{2}.u_3^{20} + \sin^2\frac{\pi\xi_2}{2}.u_3^{02} \qquad [15.B.1]$$

The stress components, expressed in series are:

$$\sigma_{11} = \cos\frac{\pi}{2}\xi_1.\sigma_{11}{}^{00} + \sin^2\frac{\pi}{2}\xi_1.\cos\frac{\pi}{2}\xi_1.\sigma_{11}{}^{20} + \cos\frac{\pi}{2}\xi_1.\sin^2\frac{\pi}{2}\xi_2.\sigma_{11}{}^{02}$$

$$\sigma_{22} = \cos\frac{\pi}{2}\xi_2.\sigma_{22}{}^{00} + \sin^2\frac{\pi}{2}\xi_1.\cos\frac{\pi}{2}\xi_2.\sigma_{22}{}^{20} + \sin^2\frac{\pi}{2}\xi_2.\cos\frac{\pi}{2}\xi_2.\sigma_{22}{}^{02}$$

$$\sigma_{33} = \sigma_{33}{}^{00} + \sin^2\frac{\pi}{2}\xi_1.\sigma_{33}{}^{20} + \sin^2\frac{\pi}{2}\xi_2.\sigma_{33}{}^{02} \qquad [15.B.2]$$

$$\sigma_{23} = \sin\frac{\pi}{2}\xi_2.\cos\frac{\pi}{2}\xi_2.\sigma_{23}{}^{01} + \sin^2\frac{\pi}{2}\xi_2.\cos\frac{\pi}{2}\xi_2\,\sin\frac{\pi}{2}\xi_2.\sigma_{23}{}^{21}\sin^3\frac{\pi}{2}\xi_2.\cos\frac{\pi}{2}\xi_2.\sigma_{23}{}^{03}$$

$$\sigma_{31} = \sin\frac{\pi}{2}\xi_1.\cos\frac{\pi}{2}\xi_1.\sigma_{31}{}^{10} + \sin\frac{\pi}{2}\xi_1.\cos\frac{\pi}{2}\xi_1\sin^2\frac{\pi}{2}\xi_2\,\sigma_{31}{}^{12} + \sin^3\xi_1.\cos\frac{\pi}{2}\xi_1\sigma_{31}{}^{30}$$

$$\sigma_{12} = \sin\frac{\pi}{2}\xi_1\cos\frac{\pi}{2}\xi_1\sin\frac{\pi}{2}\xi 2\cos\frac{\pi}{2}\xi_2\sigma_{12}{}^{11}$$

15B.2. ***Geometrical characteristics of displacement components u_j^{mn} and physical interpretation***

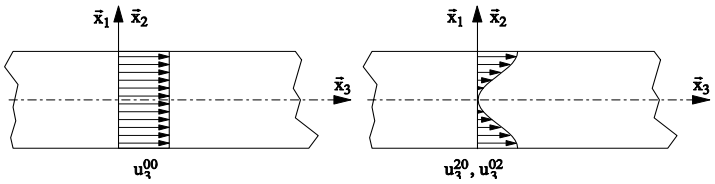

Figure 15B.1. *The three displacement components in extensional mode in a cross-section*

Axial displacement components in the series [15.B.1] are represented in Figure 15B.1. u_3^{mn} are associated with fundamental components $u_3^{00}$and with shear mode in the section (u_3^{20},u_3^{02}).

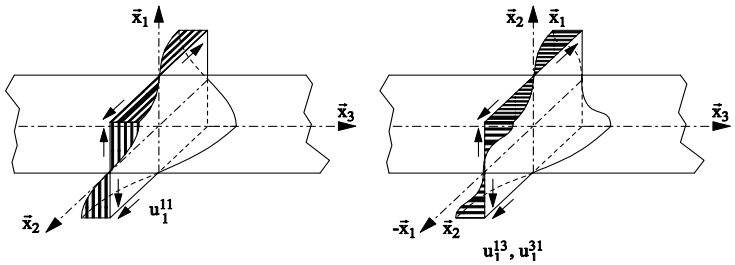

Figure 15B.2. *Higher order displacement components in the cross-section u_1^{11}, u_1^{13},u_1^{31}. u_{11} describes elementary rotation around axis $o\overrightarrow{x_1}$*

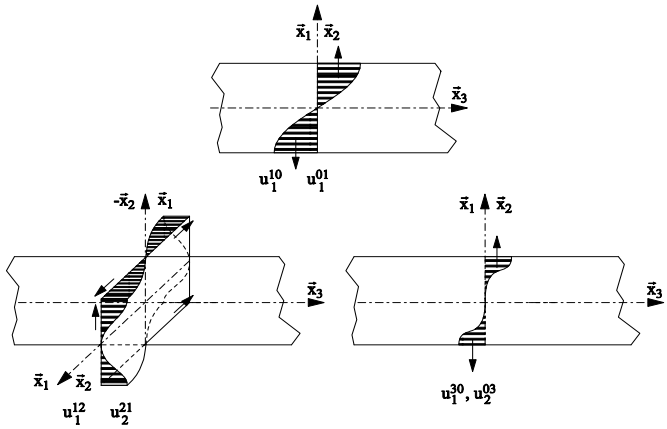

Figure 15B.3. *The three axial components in the series [15.B.1] shows shear effect in the cross-section*

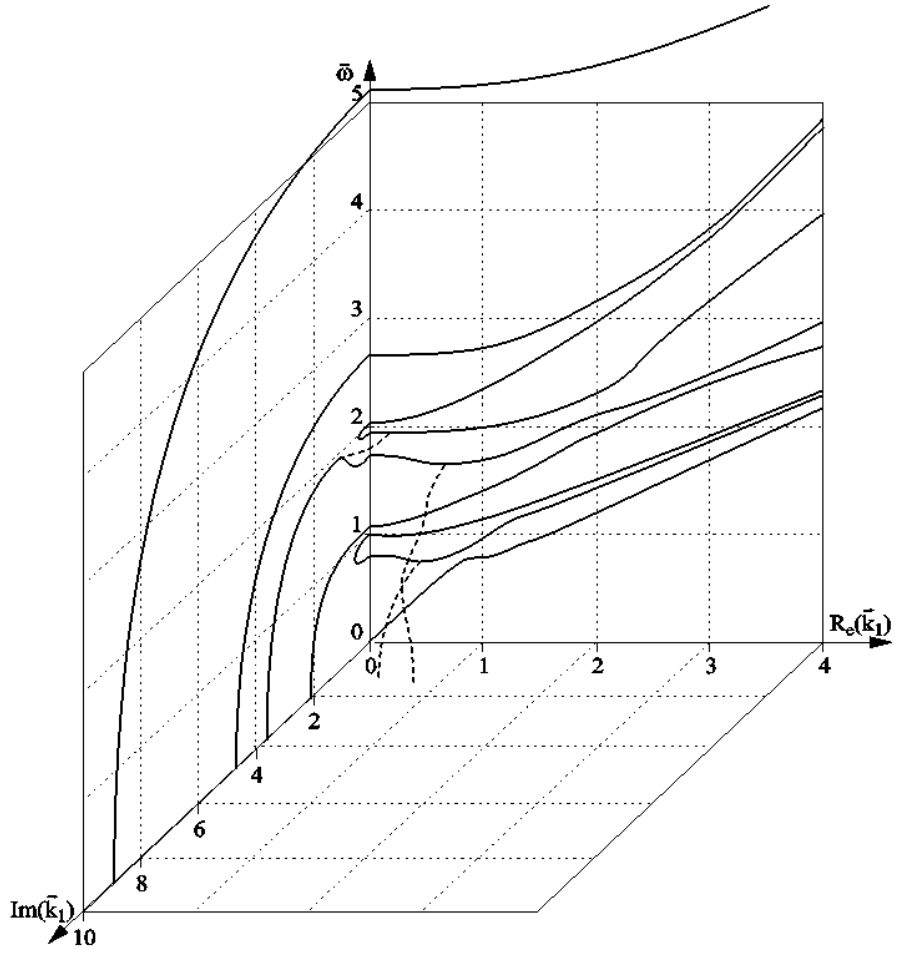

Figure 15B.4. *Frequency spectrum for nine first longitudinal modes of an isotropic rod. (Poisson's number $\nu = 0.3$) with a rectangular cross-section with flatness e = 0.5*

15B.3. *Bending mode in the direction $\overrightarrow{x_2}$ – geometrical interpretation*

Figures 15B.5, 15B.6 and 15B.7 show displacement components related to the rank of each component. Figure 15B.7 shows the frequency spectrum with nine elastodynamic modes.

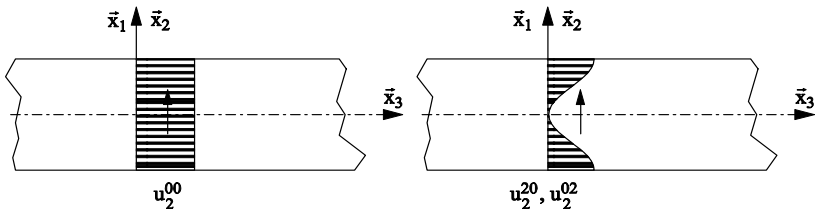

Figure 15B.5. *Bending displacement component u_2^{00} in the direction $\overrightarrow{x_2}$. The second components in the series [15.B.1] are associated with the fundamental motion in the direction $\overrightarrow{x_2}$*

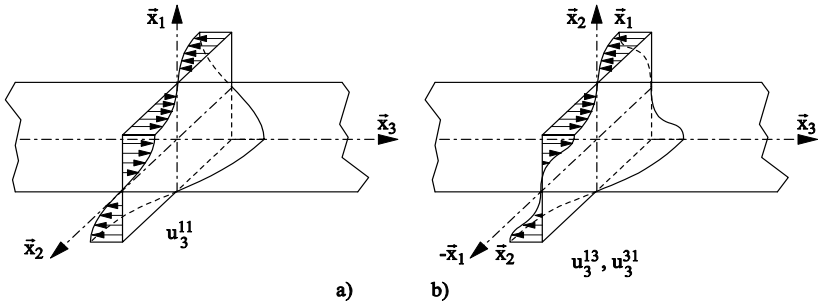

Figure 15B.6. *(a) Bending displacement component u_3^{11} describes the elementary rotation of the section around axis $o\overrightarrow{x_1}$ (b) motion of higher order u_3^{13}, u_3^{31} create tension in the cross-section*

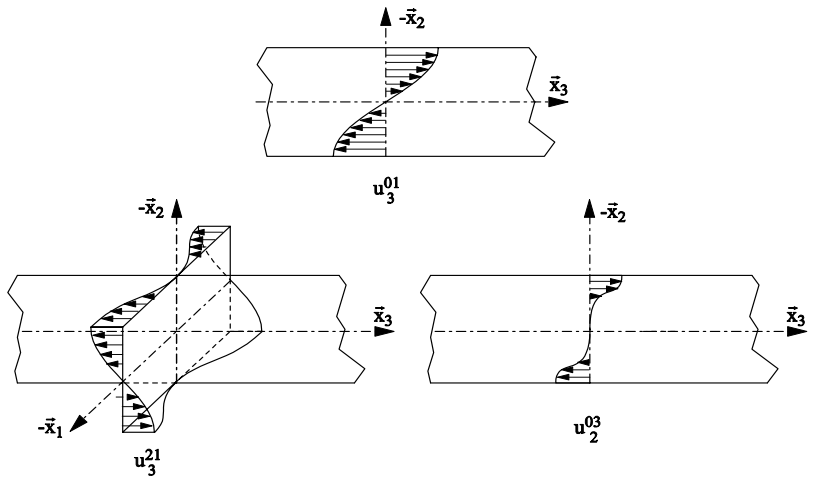

Figure 15B.7. *Bending motion: longitudinal components u_3^{01}, u_3^{21} and u_3^{03} describe the shear effect*

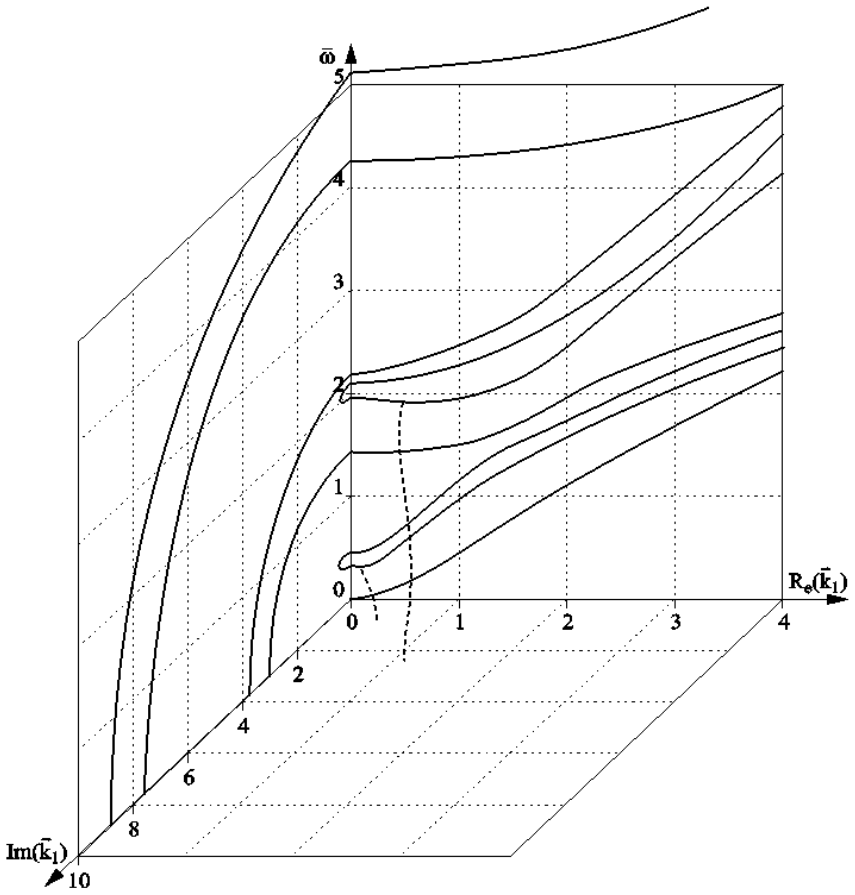

Figure 15B.8. *Frequency spectrum for bending elastodynamic modes. Rectangular cross-section; isotropic material $\nu = 0.3$; flatness $e = a_1/a_2 = 0.5$*

15B.4. *Shear motion around longitudinal rod axis*

Series expansion for torsion motion requires that the radial components be symmetrical to x_1,x_2. Longitudinal components u_3 are anti-symmetric with respect to lateral coordinates x_1,x_2. The dissymmetry of the axial components describes the warping effect of the section.

15B.4.1. *Geometrical representation of some displacements*

Figures 15B.9 and 15B.10 show various components in torsion motion.

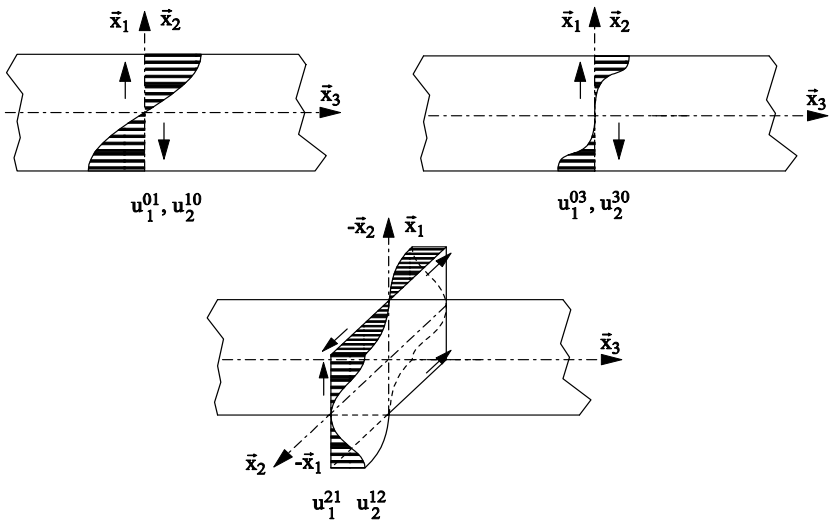

Figure 15B.9. *Displacement components in the three directions: 1, 2 and 3 in torsion mode*

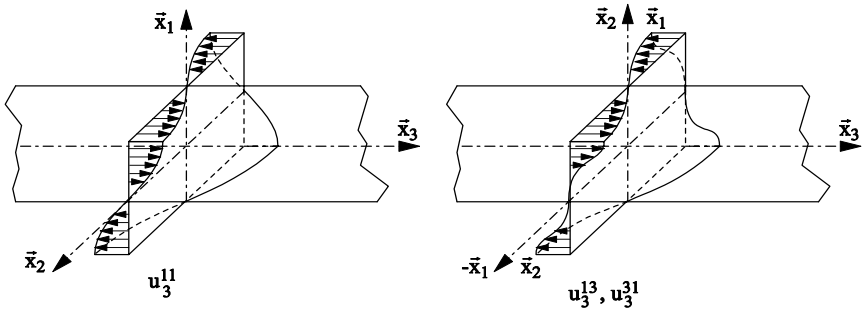

Figure 15B.10. *Displacement components in torsion are coupled with modes due to warping of the cross-section*

The shear frequency spectrum, as for extensional and bending motion, is obtained by solving with displacement components and stress components expressed as progressive waves, such that:

$$\det[\, Z_{ij}^{t} \,] = 0 \qquad [15B.3]$$

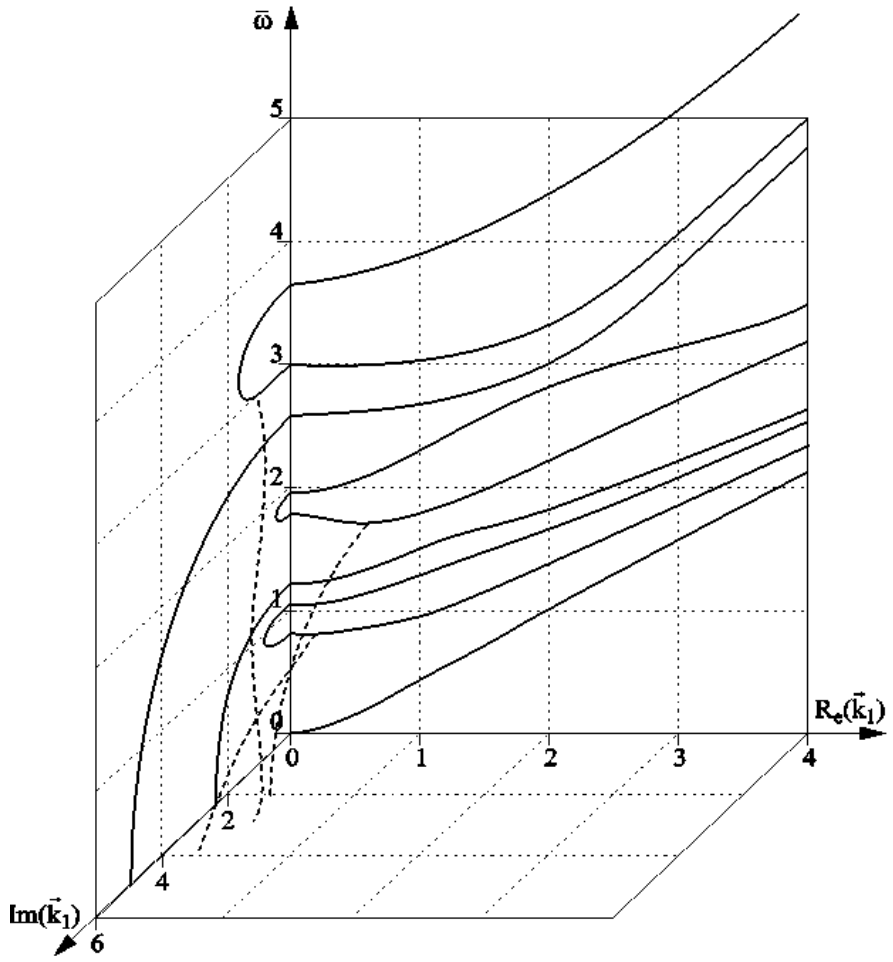

Figure 15B.11. *Frequency spectrum of nine first torsional modes; isotropic material with $\nu = 0.3$; rectangular cross-section with flatness $e = a_2/a_1 = 0.5$*